Zircon Petrochronology of Au-Rich Porphyry and Epithermal Deposits in the Golden Quadrilateral (Apuseni Mountains, Romania)

Markovic, Sava; Brunner, Manuel; Müller, Lukas; Peytcheva, Irena; Guillong, Marcel; Chelle-Michou, Cyril; Kouzmanov, Kalin; Gallhofer, Daniela; Heinrich, Christoph A.; von Quadt, Albrecht

How to cite

MARKOVIC, Sava et al. Zircon Petrochronology of Au-Rich Porphyry and Epithermal Deposits in the Golden Quadrilateral (Apuseni Mountains, Romania). In: Economic geology and the bulletin of the Society of Economic Geologists, 2024, vol. 119, n° 4, p. 967–988. doi: 10.5382/econgeo.5073

This publication URL: https://archive-ouverte.unige.ch/unige:187751
Publication DOI: 10.5382/econgeo.5073

Economic Geology, v. 119, no. 4, pp. 967–988

Zircon Petrochronology of Au-Rich Porphyry and Epithermal Deposits in the Golden Quadrilateral (Apuseni Mountains, Romania)

Sava Markovic,[1,†] Manuel Brunner,[1,2] Lukas Müller,[1,3] Irena Peytcheva,[1,4] Marcel Guillong,[1] Cyril Chelle-Michou,[1] Kalin Kouzmanov,[5] Daniela Gallhofer,[1,6] Christoph A. Heinrich,[1,7] and Albrecht von Quadt[1]

[1]*Institute of Geochemistry and Petrology, Swiss Federal Institute of Technology (ETH Zürich), Zürich 8092, Switzerland*

[2]*Kanton Zürich, Amt für Abfall, Wasser, Energie und Luft, Zürich 8090, Switzerland*

[3]*Impergeologie AG, St. Gallen 8888, Switzerland*

[4]*Geological Institute, Bulgarian Academy of Science, Sofia, Bulgaria*

[5]*Department of Earth Sciences, University of Geneva, Geneva 1205, Switzerland*

[6]*Institute for Earth Sciences, University of Graz, Graz 8010, Austria*

[7]*Faculty of Mathematics and Natural Sciences, University of Zürich, Zürich 8092, Switzerland*

Abstract

The Golden Quadrilateral of the Apuseni Mountains (Romania) represents the richest Au(-Cu-Te) porphyry and epithermal district of Europe and the Western Tethyan metallogenic belt. The Au(-Cu-Te) mineralization is associated with Neogene calc-alkaline magmatism along graben structures growing during the late stages of the Alpine-Carpathian orogeny. We use zircon petrochronology to study the time-space distribution, sources, composition, and timescales of the Au(-Cu-Te)-mineralizing magmatism and explore its link to regional tectonics. Our own and published U-Pb zircon ages document ore-forming magmatic activity between ~13.61 and 7.24 Ma. In combination with available paleomagnetic data, the new zircon ages corroborate the hypothesis that the magmatism in the Golden Quadrilateral evolved in a tectonic environment dominated by major (up to 70°) crustal block rotation. Hafnium isotope composition of Neogene zircon (ε_{Hf} between –2 and 10) supports the predominant origin of the magmas from a heterogeneous lithospheric mantle, which may have been fertilized during an earlier Cretaceous subduction event and possibly by concurrent Miocene subduction. Xenocrystic zircon shows involvement of crustal sources resembling European continental basement. Fertility indicators, including Eu/Eu* and oxygen fugacity based on zircon composition, show no systematic correlation with the mineralizing events and/or age. High-precision (isotope dilution-thermal ionization mass spectrometry) U-Pb zircon geochronology demonstrates that the magmatic systems exposed at district scale evolved over less than ~100 k.y. and that durations of hydrothermal mineralization pulses were even shorter.

Introduction

Gold and copper in magmatic-hydrothermal deposits are hosted by shallow porphyry intrusions and epithermal vein systems but sourced from much larger cooling and fluid-exsolving magma reservoirs originating in the mantle and evolving from the lower to upper crust (Hedenquist and Lowenstern, 1994; Mungall, 2002; Sillitoe, 2010). Mantle melting and evolution of mineralizing magmas is commonly caused by concurrent subduction in active arc settings but may, in some cases, have been prepared by million-years-older subduction events (Richards, 2009; Pettke et al., 2010). Over the last decade, researchers have used zircon to gain a quantitative understanding of the factors controlling the ore-forming potential of magmas, including their source composition and timescales of geochemical and thermal evolution (e.g., von Quadt et al., 2011; Chelle-Michou et al., 2014, 2017; Loucks, 2014; Buret et al., 2016; Lu et al., 2016; Rezeau et al., 2016; Tapster et al., 2016; Li et al., 2017; Large et al., 2018, 2020, 2021). Unlike major rock-forming minerals, zircon is largely immune to hydrothermal alteration, making its chemistry a reliable proxy of magmatic conditions (e.g., Fu et al., 2009).

[†]Corresponding author: e-mail, sava.markovic@erdw.ethz.ch

Zircon petrochronology combines petrogenetic information of trace element and isotopic composition with U-Pb geochronology based on variably precise dating methods such as in situ laser ablation-inductively coupled plasma-mass spectrometry (LA-ICP-MS) and secondary ion mass spectrometry (SIMS) or bulk-grain chemical abrasion-isotope dilution-thermal ionization mass spectrometry (CA-ID-TIMS; e.g., Engi et al., 2017, and references therein; Schaltegger and Davis, 2017; Schoene and Baxter, 2017). When these single-crystal methods are applied to suites of magmatic rocks in clear field relationship to ore deposits, they can provide important constraints on the source(s), as well as cooling and differentiation histories of mineralizing magmas at depth prior to porphyry intrusion and hydrothermal ore deposition (Chelle-Michou et al., 2014; Buret et al., 2016, 2017; Large et al., 2021; Nathwani et al., 2021). Moreover, zircon trace element compositions (Eu_N/Eu_N^*, Th/U, Yb/Dy, and calibrated proxies of oxygen fugacity) have even been applied to porphyry copper systems to discriminate inherently fertile from common barren magmas (e.g., Lu et al., 2016, 2017; Lee et al., 2017, 2021).

Here, we apply zircon petrochronology to study the Golden Quadrilateral of the Apuseni Mountains (Romania), where

ISSN 0361-0128; doi:10.5382/econgeo.5073; 23 p.
Digital appendices are available in the online Supplements section.

Submitted: September 16, 2022 / Accepted: June 20, 2023

the calc-alkaline magmatism during the Neogene produced dozens of porphyry and epithermal deposits constituting the richest Au district of Europe and the Western Tethyan metallogenic belt (>100 Moz of Au; e.g., Udubaşa et al., 2001; Vlad and Orlandea, 2004; Baker, 2019). The Au(-Cu-Te) ore district of the Golden Quadrilateral is thought to be caused by calc-alkaline magmatism sourced in a mantle that may have been metasomatized during both an earlier Mesozoic and a contemporaneous Neogene subduction event (e.g., Roşu et al., 1997, 2001, 2004a, b; Panaiotu, 1998; Seghedi, 2004; Neubauer et al., 2005; Harris et al., 2013; Holder, 2015; Nimis and Omenetto, 2015; Ene, 2020; Seghedi et al., 2022). We compiled an extensive zircon data set from Au-rich porphyry and epithermal deposits in the Golden Quadrilateral to explore the relationship between the Neogene magmatic activity, regional tectonic evolution, and mineralization.

Geologic Setting of the Golden Quadrilateral

The Golden Quadrilateral in Romania is a Neogene ore district located in the southern Apuseni Mountains, the island-like orogen embayed by the Carpathian arc (see Fig. 1; Schmid et al., 2008, 2020; Ustaszewski et al., 2008; Kounov and Schmid, 2013; van Hinsbergen et al., 2020). On a global scale, the Golden Quadrilateral is a small segment of the 3,500-km-long Western Tethyan metallogenic belt, which stretches from Slovakia to Turkey and hosts numerous volcanogenic massive sulfide, porphyry, and epithermal deposits of predominantly Cretaceous to Cenozoic age (e.g., Janković, 1997; Richards, 2015; Baker, 2019).

The porphyry and epithermal deposits in the Golden Quadrilateral are particularly rich in Au and Te and are confined to three sediment-filled Miocene grabens (i.e., basins): (1) the NW- to SE-trending Brad-Săcărâmb, (2) the WNW- to ESE-trending Zlatna, and (3) the small Roşia-Bucium basin in the northern part of the district (see Fig. 1; e.g., Ghitulescu and Socolescu, 1941; Udubaşa et al., 2001; Cook and Ciobanu, 2004; Vlad and Orlandea, 2004; Baker, 2019). These basins host, among others, the largest epithermal Au deposit of the Western Tethyan belt (Roşia Montană), one of Europe's richest Cu-Au porphyries (Roşia Poieni), historically important mining centers (Deva, Barza, Valea Morii, Săcărâmb, Zlatna, Baia de Arieş), and several recent exploration camps (Ivascanu et al., 2003; Kouzmanov et al., 2003, 2005, 2007; Milu et al., 2003, 2004; Vlad and Orlandea, 2004; Baker, 2019). More recently discovered Au-Cu mineralization, which is the focus of this study, includes the following: (1) the Au-Ag epithermal deposit Certej, Au-Cu porphyry deposits at Bolcana, Cireşata, Colnic, and Rovina, all hosted within the Brad-Săcărâmb basin, (2) the Au-Cu porphyry deposits at Stănija and Ciungi Stănija in the western part of the Zlatna basin, and (3) the porphyry-Au occurrences at Geamăna West, Bucium South, and Poeniţa, in the Roşia-Bucium basin (see Fig. 1). Gold and Cu grades are associated with disseminated and vein sulfides (chalcopyrite-bornite-pyrite ± molybdenite in porphyry, and additional sphalerite-galena-pyrrhotite-arsenopyrite Cu-Pb sulfosalts in epithermal veins) hosted in the Neogene intrusions and/or adjacent Cretaceous and Cenozoic sedimentary rocks (Table 1 with references; App. Table A1).

The mineralized intrusions of the Golden Quadrilateral pierce the southern part of the Cretaceous-age Apuseni orogen, which was assembled mainly from pre-Mesozoic basement units (Dacia and Tisza megablocks) and their Mesozoic cover, ophiolite nappes derived from Jurassic ocean basins and oceanic arcs, and intruding calc-alkaline rocks of the Apuseni-Banat-Timok-Srednogorie belt (e.g., Săndulescu, 1984; Dallmeyer et al., 1999; Bortolotti et al., 2002, 2004; Pană et al., 2002; Nicolae and Saccani, 2003; Seghedi, 2004; Márton et al., 2007; Zimmerman et al., 2008; Balintoni et al., 2009; Dunkl et al., 2009; Gallhofer et al., 2017; Reiser et al., 2017). The latter is a magmatic arc related to the then N-dipping subduction of the Neotethys (Eastern Vardar) ocean that during the Mesozoic separated the Africa-derived microplate Adria from Europe-derived Tisza and Dacia megaunits in front of the European craton (Moesia block sensu lato; e.g., Schmid et al., 2008, 2020; van Hinsbergen et al., 2020). The subduction of Neotethys during Late Cretaceous to Paleogene times gave rise to major porphyry-related ore deposits including Majdanpek, Bor, and the Srednegorie district farther toward the south and east (e.g., Janković, 1997; Berza et al., 1998; Ciobanu et al., 2002; von Quadt et al., 2005; Gallhofer et al., 2015). During the Neogene (Late Miocene to Pliocene), the Apuseni orogen was overprinted by block rotation and extension, resulting in NW-SE–oriented graben structures filled by siliciclastic sedimentary rocks, marls, and freshwater limestones and a variety of volcanic rocks and subvolcanic intrusions associated with the hydrothermal deposits of the Golden Quadrilateral (see Ghitulescu and Socolescu, 1941; Ianovici et al., 1969; Merten et al., 2011, and references therein).

The porphyry-type and epithermal Au(-Cu-Te) mineralization in the Golden Quadrilateral is related to an ~7-m.y.-long phase of postorogenic calc-alkaline magmatism (Lemne, 1983; Pécskay et al., 1995; Roşu et al., 1997, 2001, 2004a, b; Kouzmanov et al., 2005, 2007; Holder, 2015; Ene, 2020). Besides shallow (<1.5 km) mineralized porphyries, this magmatic event produced barren intrusions, extensive pyroclastic deposits, and lava flows (e.g., Ianovici et al., 1969; Vlad and Orlandea, 2004). The magmatic rocks are predominantly andesitic in composition, containing abundant hornblende and biotite, but also including subordinate basaltic andesites, dacites and rhyolites, and rare pyroxene- and garnet-bearing trachybasalts and trachyandesites (e.g., Seghedi, 2004; Seghedi et al., 2022). Apatite, zircon, Fe-Ti oxides, and Cr spinel make up the most common accessory phases (Seghedi, 2004). The majority of the Neogene intrusions in the Golden Quadrilateral exhibit uniform calc-alkaline arc-like signatures—i.e., enrichment in large ion lithophile elements (LILEs), depletion in high field strength elements (HFSEs) and Ti and Nb, and steep light rare earth element (LREE) to heavy rare earth element (HREE) profiles (e.g., Roşu et al., 2004a; Harris et al., 2013; Seghedi et al., 2022). However, a few smaller magmatic centers, located mainly in the Roşia-Bucium basin, show more alkaline compositions, characteristic of extension-related mantle melting and in line with geophysical evidence for thinned crust below the northern, most extended part of the graben structures (Takács et al., 1996; Seghedi, 2004; Bala et al., 2017). Sporadic adakite-like intrusions, indicative of lower-crustal fractionation, are confined to the southeastern segment of the Brad-Săcărâmb basin and Deva (Rosu et al., 2004a; Harris et al., 2013).

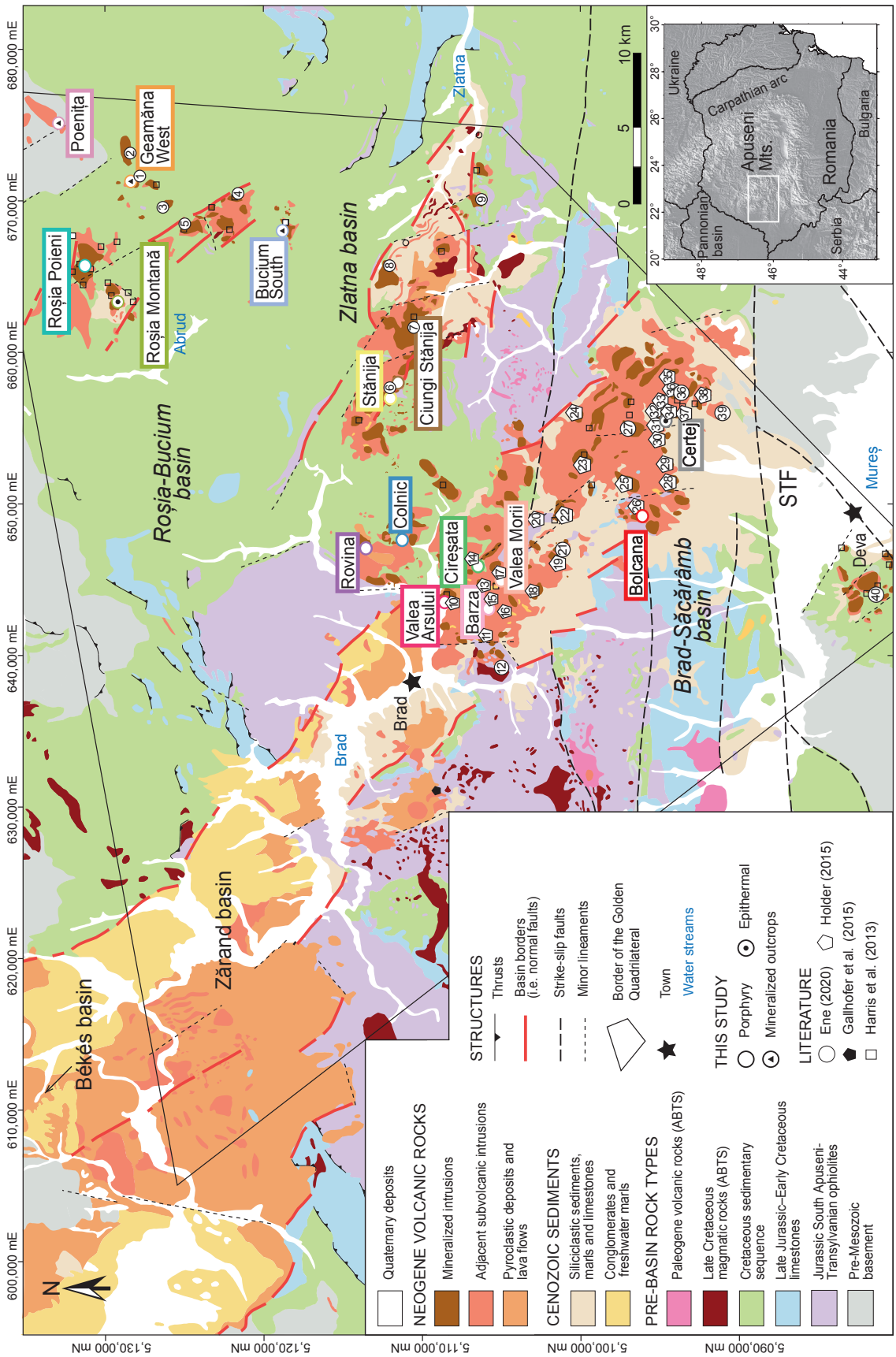

Fig. 1. Geologic map of the Golden Quadrilateral district in the southern Apuseni Mts. (modified after Roșu, 2001). Mineralized porphyry stocks intrude the basement and sedimentary sequences along the Brad-Săcărâmb, Zlatna, and Roșia-Bucium volcano-sedimentary basins. Samples of Harris et al. (2013), Gallhofer et al. (2015), Holder (2015), and Ene (2020) are included in the compilation of whole-rock geochemical data and U-Pb zircon ages. Inset: Relief map of Romania showing the location of the Golden Quadrilateral within the Carpathian orogen. Numbered localities in the Roșia-Bucium basin: 1 = Geamăna West, 2 = Geamăna East, 3 = Detunata, 4 = Poienile-Stâlnișoara, 5 = Dealul Contu; in the Zlatna basin: 6 = Corbu Stream/Stănija, 7 = Almașu Mare/Neagra quarry, 8 = Trâmpoiele, 9 = Măgura Lupului quarry; in the Brad-Săcărâmb basin: 10 = Valea Arsului/Arsului, 11 = Curatu, 12 = Dealul Fetii, 13 = Arisor, 14 = Cireșata, 15 = Barza Nouă, 16 = Smereciu, 17 = Valea Morii, 18 = no given name in literature, 19 = Câinel, 20 = Hărtăgani, 21 = Câinenii Marii, 22 = Stirba, 23 = Cetraș, 24 = Buha, 25 = Stogu, 26 = Bolcana, 27 = Coasta Mare/Hondol-Măceriș, 28 = Fairag, 29 = Fairagut, 30 = Hondol Neckul, 31 = Hondol, 32 = Baiaga, 33 = Delul Grozii, 34 = Delul Grozii Sur, 35 = Frasinata, 36 = Haiău, 37 = Sarcău, 38 = no given name in literature, 39 = Ledișoiu; in the southernmost part of the Golden Quadrilateral: 40 = Deva. ABTS = Apuseni-Banat-Timok-Srednogorie, STF = South Transylvanian fault.

Table 1. Summary of the Studied Au-Rich Porphyry and Epithermal Deposits in the Golden Quadrilateral

Deposit	Type	Project stage	Resource category	Ore tonnage (Mt)	Au grade (g/t)	Cu grade (%)	Au (Moz)	Cu (t)	References
Bolcana	Au-Cu porphyry	Advanced exploration	Inferred	381.0	0.53	0.18	6.49	686,000	Milu et al. (2003), Cardon et al. (2005, 2008), Cioacă et al. (2014), Dénes et al. (2014), Ivascanu et al. (2019), Tusa et al. (2019), Eldorado Gold (2020), Blannin et al. (2021)
Certej	Au-Ag epithermal	Development	Indicated + measured	88.0	1.35	-	3.83	-	Gál et al. (2010), Alexander et al. (2014), Apopei et al. (2014a, b, 2016), Eldorado Gold (2020)
			Inferred	0.8	0.86	-	0.02	-	
Cireşata	Au-Cu porphyry	Advanced exploration	Indicated + measured	154.4	0.77	0.15	3.82	233,600	Halga et al. (2010), PEG Mining Consultants Inc. (2010), AGP Mining Consultants Inc. (2012, 2019), Ruff et al. (2012), Rocha (2013), Ruff (2013), New Senet (PTY) Ltd. (2021)
Colnic	Au-Cu porphyry	Advanced exploration	Measured	29.1	0.65	0.12	0.61	33,566	Halga et al. (2010), PEG Mining Consultants Inc. (2010), AGP Mining Consultants Inc. (2012, 2019), Ruff (2013), New Senet (PTY) Ltd. (2021)
			Indicated	97.5	0.49	0.10	1.53	95,254	
			Inferred	1.6	0.41	0.09	0.02	1,361	
Rovina	Au-Cu porphyry	Advanced exploration	Measured	33.1	0.36	0.29	0.38	96,162	PEG Mining Consultants Inc. (2010), AGP Mining Consultants Inc. (2012, 2019), Ruff (2013), New Senet (PTY) Ltd. (2021)
			Indicated	78.1	0.26	0.22	0.66	171,911	
			Inferred	16.0	0.18	0.19	0.09	29,937	
Stănija	Au-Cu porphyry	Prospect	-	-	-	-	-	-	P. Ivăşcanu (pers. commun., 2016), R. Ruff (pers. commun., 2018)
Ciungi Stănija	Au-Cu porphyry	Prospect	-	-	-	-	-	-	P. Ivăşcanu (pers. commun., 2016), R. Ruff (pers. commun., 2018)

Dashes in otherwise-empty cells indicate no data provided

The calc-alkaline compositions in the Golden Quadrilateral may be related to one or two subduction events in the Carpathian region. The Golden Quadrilateral magmas may have formed by postsubduction extensional melting of a lithospheric mantle modified by earlier subduction processes, which may have started in the Jurassic (ophiolite nappes) and extended to the Late Cretaceous (Neotethys subduction and Apuseni-Banat-Timok-Srednogorie arc; Roşu et al., 2001, 2004a; Schmid et al., 2008, 2020; Harris et al., 2013; van Hinsbergen et al., 2020). Alternatively, they may represent true arc magmas associated with westward-directed subduction of the oceanic lithosphere of Alpine Tethys, preserved as relicts in the Ceahlău-Severin ophiolites and geophysically indicated by a subvertical slab below the Eastern Carpathians (Vrancea seismic zone; e.g., Linzer, 1996; Linzer et al., 1998; Mason et al., 1998; Nemcok et al., 1998; Wortel and Spakman, 2000; Sperner et al., 2002; Carminati et al., 2012; Nimis and Omenetto, 2015).

Samples and Methods

Fifty-four samples of Neogene intrusions and some basement rocks were collected from drill core and outcrops (App. Table A2). Intrusions with well-established spatial and temporal relationships to mineralization were sampled, whenever possible, from minimally altered, homogeneous rock intervals (i.e., away from fractures and intrusive contacts).

The studied Neogene intrusions are markedly uniform in their mineralogy. The majority correspond to andesites containing varying proportions of plagioclase, hornblende, and biotite phenocrysts embedded in a plagioclase-rich groundmass. Common accessory phases observed both in thin section and mineral separates include apatite, zircon, and magnetite. Groundmass quartz occurs as a minor phase (<5 vol %) in few andesite samples, while quartz phenocrysts (<2 mm) are only present in the host-rock dacites at Bolcana (sample SMB-12) and Roşia Montană (RM19) among the Neogene samples, in Jurassic basement rhyolites from Bolcana and Certej (SMB-22, A17-19, and A17-23), and in regional samples of Mesozoic granitoids (DG072, DG115, DG109, DG101, DG091, DG112, DG100, and DG110; Gallhofer et al., 2015, 2017). More mafic rocks, including syenites, basalts, and gabbros corresponding to the Jurassic ophiolites, were sampled from drill core at Certej (A17-13 and A17-17) and outcrops in the broader area of the southern Apuseni Mountains (Gallhofer et al., 2017). Because of the petrographic uniformity of the Neogene intrusions, the nomenclature used in exploration was favored over the petrographic names in the text; both are provided in Appendix Table A2.

Designations pre-, syn-, and postmineralization denote the relative timing of the emplacement of the Neogene intrusions with respect to the bulk of the mineralization. These are adopted from exploration and updated with our observations and rely on deposit-scale core logging and assay results. Intrusions denoted as premineralization host the earliest, barren A-type quartz veins but never truncate sulfide-bearing veins or higher-grade disseminated mineralization. Synmineralization

intrusions both host and crosscut sulfide veins and elevated metal grades. Postmineralization intrusions crosscut higher-grade zones and carry significantly lower grades compared to the pre- and synmineralization intrusions or are fully barren. Host-rock intrusions predate the premineralization porphyries based on crosscutting relationships. The term "unclear" is used for those intrusions whose spatial and temporal relationship to mineralization could not be established with confidence.

Sample aliquots for whole-rock geochemistry were mixed with an Li-based fluxer (66% Li tetraborate and 34% Li metaborate) in 1:5 proportion to produce glass beads. Major element oxide concentrations were analyzed on the glass beads using a wavelength-dispersive spectroscopy (WDS) Panalytical Axios X-ray fluorescence (XRF) instrument. Trace element concentrations were analyzed with a 115-µm spot size on an Excimer laser system coupled to a NexION 2000 quadrupole inductively coupled plasma-mass spectrometer. Data reduction was done using the MATLAB-based software SILLS (Guillong et al., 2008), with CaO concentrations measured by XRF serving as internal standard.

Zircon crystals were concentrated in a procedure including rock disintegration using the high-voltage pulse system SelFrag, sieving, processing on a Franz magnetic separator, density separation with methylene iodide, and picking under a binocular. The zircon crystals were heated in a muffle furnace at 900°C for 48 h to anneal radiation-damaged domains prior to their removal by leaching (chemical abrasion; Mattinson, 2005; von Quadt et al., 2014), embedded in epoxy mounts, ground, and polished. Cathodoluminescence (CL) imaging of the internal texture of zircon crystals was carried out on a JEOL JSM-6390 scanning electron microscope (SEM) equipped with a Deben Centaurus panchromatic CL detector.

Uranium-lead isotope ratios and trace element concentrations were analyzed simultaneously in situ on the same zircon volumes using a S155-LR ASI Resolution Excimer laser ablation system coupled to a Thermo Scientific Element-XR sector field inductively coupled plasma-mass spectrometer. The analyses were carried out with a laser spot size of 29 µm at a repetition rate of 5 Hz and a fluence of 2 J cm^{-2}. Raw output data were processed with the IgorPro-based Iolite v3.6 software (Paton et al., 2010, 2011), and signal treatment was done utilizing the VizualAge software package (Petrus and Kamber, 2012). During signal treatment, analyses with unstable age signals longer than one-third of the integration time were discarded, whereas shorter unstable age signals and those with anomalous common Pb and Al, P, Ti, and La intensities (indicative of mineral/melt inclusions) were filtered out. Individual $^{206}Pb/^{238}U$ dates were corrected for initial $^{230}Th/^{238}U$ disequilibrium in the ^{238}U-^{206}Pb decay scheme by employing a Th-U mineral-melt partition coefficient of 0.2 (Wotzlaw et al., 2014). Weighted mean ^{206}Pb-^{238}U dates were calculated using IsoplotR (Vermeesch, 2018) and are reported with the associated 2σ statistical uncertainty (95% confidence level) and external uncertainty that includes a 1.5% excess intersession variance of the measured U/Pb and Pb/Pb in the secondary zircon standard AUSZ7-5 (Horstwood et al., 2016; von Quadt et al., 2016).

Trace element concentrations in zircon were quantified using the stoichiometric concentration of Si in zircon of 15.2 wt % as the internal standard. Titanium concentrations were corrected relative to the 91500 zircon reference material (Szymanowski et al., 2018). Zircon Eu_N/Eu_N^* for the ore-related Neogene intrusions and Jurassic basement rocks were calculated relative to the concentrations of Eu, Sm, and Gd in C1 chondrite by McDonough and Sun (1995). Ti-in-zircon crystallization temperatures and melt oxygen fugacity relative to the fayalite-magnetite-quartz buffer (ΔFMQ) were calculated from trace element concentrations (Ti, Ce, U) after the calibration of Loucks et al. (2020), assuming a fixed lithostatic pressure of 200 MPa and a_{TiO_2}= 0.75 for all studied samples, and a_{SiO_2}= 0.7 or a_{SiO_2}= 1 for quartz-free or rocks containing magmatic quartz, respectively. Variation in intensive parameters a_{TiO_2} and a_{SiO_2} and water content during differentiation are not accounted for in our calculations, and our discussion in the following is solely based on empirical observations.

Hafnium isotope composition of zircon was analyzed on the same spots ablated for U-Pb geochronology or adjacent on domains with similar CL appearance. The analyses were carried out on an ASI Resolution ArF Excimer laser ablation system coupled to a Nu Plasma 2 multicollector-inductively coupled plasma-mass spectrometer, employing a 50-µm laser spot size, repetition rate of 5 Hz, and a fluence of 4 J cm^{-2}. The data were processed with the IgorPro-based Iolite v3.5 software using an in-house data reduction scheme. The initial zircon $^{176}Hf/^{177}Hf$ ratios and $\varepsilon_{Hf_{(t)}}$ values were calculated with the in situ U-Pb dates, ^{176}Lu decay constant of 1.867×10^{-11} $year^{-1}$ (Scherer et al., 2001), and $^{176}Hf/^{177}Hf$ and $^{176}Lu/^{177}Hf$ values of 0.282785 and 0.0336, respectively, for the chondritic uniform reservoir (CHUR; Bouvier et al., 2008).

Zircon crystals displaying homogeneous CL appearance and no inheritance detectable in reconnaissance LA-ICP-MS dating were selected for high-precision U-Pb geochronology using ID-TIMS. Following the standardized procedure, the zircon crystals were plucked out of epoxy mounts, chemically abraded in HF at 180°C for 12 h (Mattinson, 2005), cleaned in multiple cycles with HNO_3 and HCl, spiked with the ^{202}Pb-^{205}Pb-^{233}U-^{235}U EARTHTIME (ET2535) tracer solution (Condon et al., 2015; McLean et al., 2015), and dissolved in HF at 210°C within 60 h (for a detailed description of the laboratory procedure, see Wotzlaw et al., 2014). Uranium and lead were separated from the matrix elements by ion-exchange chromatography using an HCl-based single-column chemistry modified after Krogh (1973). High-precision U-Pb isotope analyses were carried out on a Thermo TRITON Plus TIMS instrument in static measurement mode, with Faraday cups connected to 10^{13} Ω amplifiers (von Quadt et al., 2016; Wotzlaw et al., 2017). Data reduction was carried out using the Tripoli and ET_Redux softwares (Bowring et al., 2011) with algorithms of McLean et al. (2011). Individual U-Pb dates were calculated relative to the published calibration of the ET2535 tracer solution (Condon et al., 2015) using the decay constants of Jaffey et al. (1971) and are reported with their 2σ uncertainties (95% confidence level).

Results

Whole-rock geochemistry

Whole-rock major and trace element compositions of the Neogene intrusions and basement rocks from the Golden

Quadrilateral are reported in Appendix Table A3. Although least altered rocks were sampled at each site, nearly all of the Neogene samples still exhibit a significant alteration overprint, which is detectable in their high loss on ignition (LOI) values (mean = 4.24 wt %). Because the original concentrations of alkali metals and silica are more likely to be disturbed by alteration, we used the classification diagrams based on immobile trace elements for our samples (Winchester and Floyd, 1977, modified by Pearce, 1996; Ross and Bédard, 2009).

The Neogene intrusions exhibit a uniform composition and geochemical affinity (Fig. 2). The majority are characterized by consistent Zr/Ti and Nb/Y ratios (Zr/Ti = 0.02–0.04 and Nb/Y = 0.32–0.57) with very limited scatter and classify as andesites and basaltic andesites (Fig. 2A). These results are consistent with their mineralogical composition and earlier data (e.g., Roşu et al., 2004a; Seghedi, 2004; Harris et al., 2013; Ene, 2020). Intrusions from Poeniţa and Geamăna West are more alkaline and plot into the trachyandesite field (Nb/Y values of 0.86 and 1.07, respectively). The host-rock intrusion from Bolcana also falls into the trachyandesite field (Nb/Y = 0.73), although it was petrographically classified as dacite, as it contains conspicuous macroscopic quartz phenocrysts. Except at Bolcana, no pronounced shift in composition was observed between successive Neogene intrusions within individual deposits. The most evolved samples in the region are the basement magmatic rocks at Bolcana and Certej, which correspond to rhyolites (Zr/Ti ~ 0.085). The least evolved rocks are basalts sampled from drill core within the ophiolite basement at Certej (Zr/Ti ~ 0.008). All our samples apart from the basalts, which are tholeiitic, display a calc-alkaline affinity (Th/Yb mean value of 2.62), with no adakite-like features as reported for a few intrusions in the Bolcana-Certej-Săcărâmb and Deva areas (Fig. 2B; e.g., Roşu et al., 2004a; Seghedi, 2004; Harris et al., 2013).

CL imaging

The imaged zircon crystals vary in size mostly between 30 and 200 µm along the c axis and occasionally reach up to ~350 µm. They are mostly bipyramidal and exhibit oscillatory zoning from core to rim (App. Fig. A1). Neogene zircons from Certej, Bolcana, Rovina, Colnic, Stănija, and Ciungi Stănija exhibit similar characteristics, and only those from Certej are depicted in Appendix Figure A1. Conversely, zircons from Geamăna West and Poeniţa display a more varied CL appearance. For

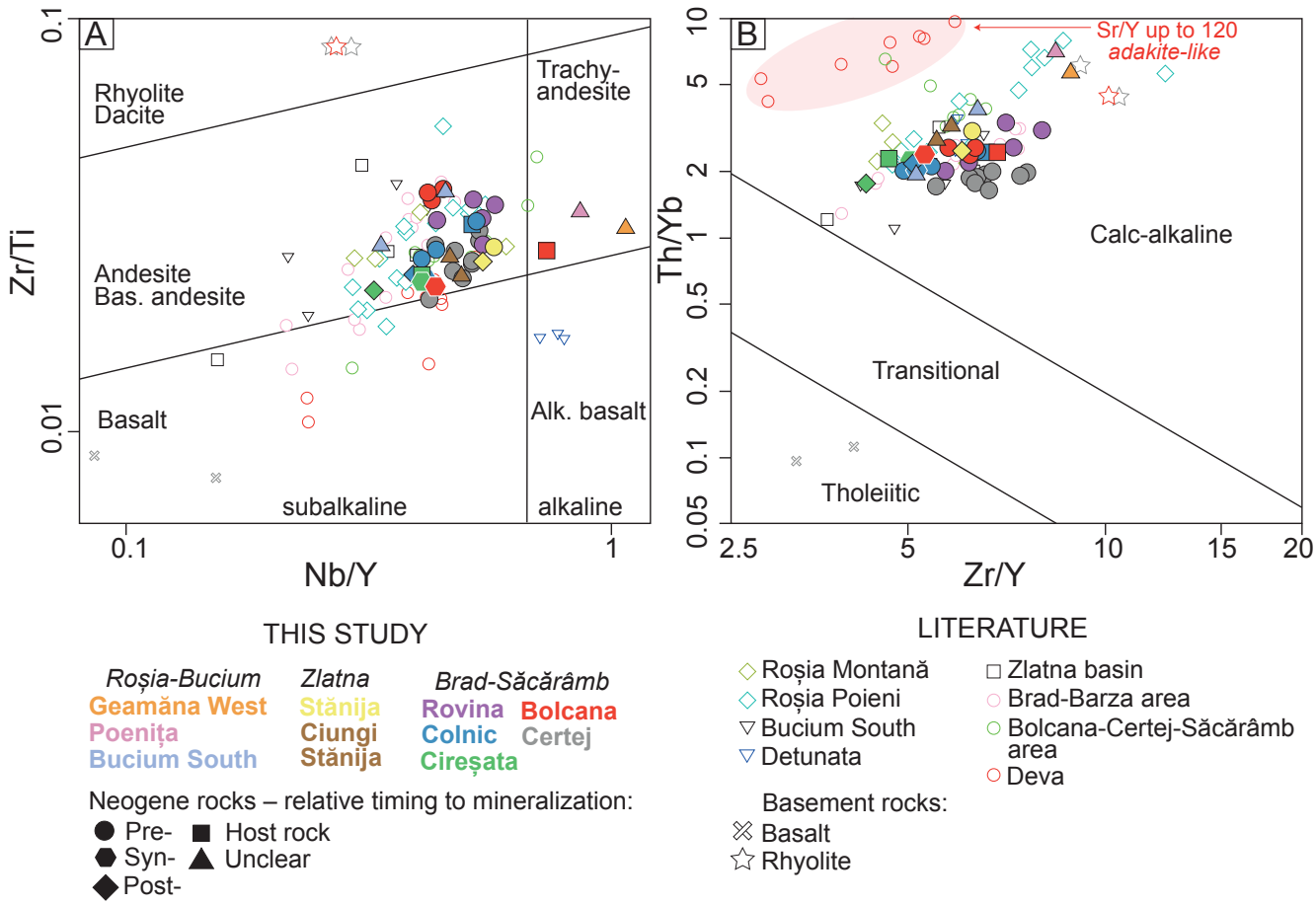

Fig. 2. A) Neogene intrusions from the Golden Quadrilateral plot predominantly in the field of basaltic andesites and andesites on the Nb/Y versus Zr/Ti classification diagram (Winchester and Floyd, 1977; modified by Pearce, 1996) and B) uniformly in the calc-alkaline field on the affinity diagram based on immobile-element ratios Zr/Y and Th/Yb (Ross and Bédard, 2009). Slightly elevated adakite-like Sr/Y ratios (<120) are observed in few samples from Deva and southeastern Brad-Săcărâmb, correlating with high Th/Yb (>5) and low Zr/Y (<6) ratios. Literature data plotted for comparison corresponds to least altered samples of Harris et al. (2013). Alk. = alkaline, Bas. = basaltic.

instance, one subpopulation from Geamăna West has bright Ordovician and Neogene cores and darker overgrowths of Triassic and Neogene age, respectively. Another subpopulation, which corresponds to the oldest, Archean-Proterozoic dates, consistently displays dark-gray to black tones from core to rim. Zircons from Poeniţa locally host euhedral bright and dark cores with inclusions and fractures, whereas those from the basement rhyolites exhibit oscillatory, sector, and patchy zoning and besides bipyramids, also appear in needle-like shapes.

In situ U-Pb zircon geochronology

Results of the in situ zircon U-Pb geochronology are reported in Appendix Table A4. The ^{230}Th-corrected ^{206}Pb/^{238}U weighted mean dates of 36 samples, encompassing the Neogene intrusions and basement rocks in the Golden Quadrilateral, are reported in Table 2 and shown in Figure 3.

The weighted mean dates of the Neogene samples fall into three time intervals. Most of the samples yield dates between ~13.2 and 12.1 Ma, which we call phase I. These include the intrusions at Bucium South (Roşia-Bucium basin), Stănija, and Ciungi Stănija (Zlatna basin), the host-rock intrusion at Bolcana, and the entire magmatic suites at Rovina, Colnic, and Certej (Brad-Săcărâmb basin). All intrusions at Cireşata and the premineralization intrusions at Bolcana yield resolvable younger dates, between ~11.5 and 10.7 Ma (phase II). The weighted mean dates of the intrusions at Geamăna West and Poeniţa (Roşia-Bucium basin) fall between ~8.2 and 7.3 Ma (phase III).

The weighted mean dates of the host-rock, pre-, syn-, and postmineralization intrusions from the individual deposits in the Golden Quadrilateral mostly overlap within the uncertainty of LA-ICP-MS. For example, in the Au-Cu porphyry deposits Colnic and Cireşata, the weighted mean

Table 2. In Situ U-Pb Zircon Weighted Mean Dates of the Neogene Intrusions and Basement Rhyolites from the Golden Quadrilateral

No.	Sample ID	Locality	Lithology	^{230}Th-corrected ^{206}Pb/^{238}U weighted mean date (Ma)	2σ abs. (Ma)	External uncertainty abs. (Ma)	n^1	MSWD[2]
1	A17-3	Geamăna West		7.42	0.13	0.17	3/37	2.84
2	A17-5	Poeniţa		8.08	0.06	0.14	18/51	0.99
3	A17-1	Bucium South		12.79	0.07	0.20	24/74	1.19
4	A17-40	Stănija	Postmineral dike	12.19	0.05	0.19	57/101	0.98
5	A17-39	Stănija	Mineralized porphyry	12.34	0.08	0.20	30/82	1.14
6	A17-4-1	Ciungi Stănija		12.35	0.12	0.22	11/28	0.28
7	A17-31	Rovina	B porphyry	12.29	0.06	0.19	57/75	1.09
8	A17-33	Rovina	Intrusive magmatic breccia (IMB)	12.16	0.06	0.19	31/91	1.07
9	A17-32	Rovina	Glam breccia	12.34	0.06	0.19	49/85	1.06
10	A17-34	Rovina	C 2 porphyry	12.38	0.07	0.20	38/63	1.36
11	A17-35	Rovina	C 1 poprhyry	12.43	0.06	0.20	59/79	1.34
12	A17-25	Colnic	Postmineral dike	12.30	0.08	0.20	25/55	1.43
13	A17-37	Colnic	Colnic 1 porphyry	12.39	0.05	0.19	42/96	1.23
14	A17-26	Colnic	Late-mineral dike	12.41	0.08	0.20	21/52	0.84
15	A17-27	Colnic	Wall-rock porphyry	12.29	0.06	0.19	36/91	1.34
16	A17-24	Colnic	Colnic 2 porphyry	12.21	0.12	0.22	18/56	1.87
17	A17-28	Colnic	F2 Hill porphyry	12.67	0.09	0.21	17/42	0.54
18	A17-38	Cireşata	Wall-rock porphyry	11.32	0.04	0.17	70/101	1.06
19	A17-29	Cireşata	Early-mineral porphyry	11.25	0.05	0.18	48/74	1.08
20	A17-29	Cireşata	Intermineral porphyry	11.34	0.07	0.18	25/35	0.87
21	A17-30	Cireşata	Late-postmineral dike	11.32	0.05	0.18	53/76	1.11
22	SMB-3a	Bolcana	Crowded amp-bt porphyry 1	11.14	0.08	0.19	27/38	0.93
23	SMB-3b	Bolcana	Crowded amp-bt porphyry 2	10.77	0.17	0.23	11/25	1.96
24	SMB-11a	Bolcana	Shell porphyry	11.14	0.11	0.20	11/22	0.97
25	SMB-12	Bolcana	Host-rock porphyry	13.01	0.06	0.20	40/45	1.04
26	SMB-22	Bolcana	Rhyolite	158.63	0.66	2.47	36/55	1.37
27	A17-22	Certej	Hondol-shallow porphyry	12.49	0.05	0.19	51/77	1.17
28	A17-16	Certej	Hondol-deep porphyry	12.59	0.05	0.20	62/84	0.95
29	A17-9	Certej	Hondol-Magura porphyry	12.61	0.06	0.20	42/83	1.49
30	A17-15	Certej	Baiaga-Nose porphyry	12.53	0.07	0.20	38/74	1.42
31	A17-18	Certej	Baiaga porphyry	12.68	0.06	0.20	31/52	1.25
32	A17-12	Certej	Transitional 1 porphyry	12.57	0.06	0.20	36/81	0.88
33	A17-10	Certej	Transitional 2 porphyry	12.58	0.05	0.20	45/68	1.31
34	A17-14	Certej	Grozii 1 porphyry	12.65	0.05	0.20	45/88	0.90
35	A17-11	Certej	Grozii 2 porphyry	12.66	0.05	0.20	40/59	1.15
36	A17-19	Certej	Rhyolite	156.74	0.60	2.43	28/80	1.43

Abbreviations: amp = amphibole, bt = biotite

[1]Number of analyses included in date calculation/total number of analyses

[2]Mean square weighted deviation

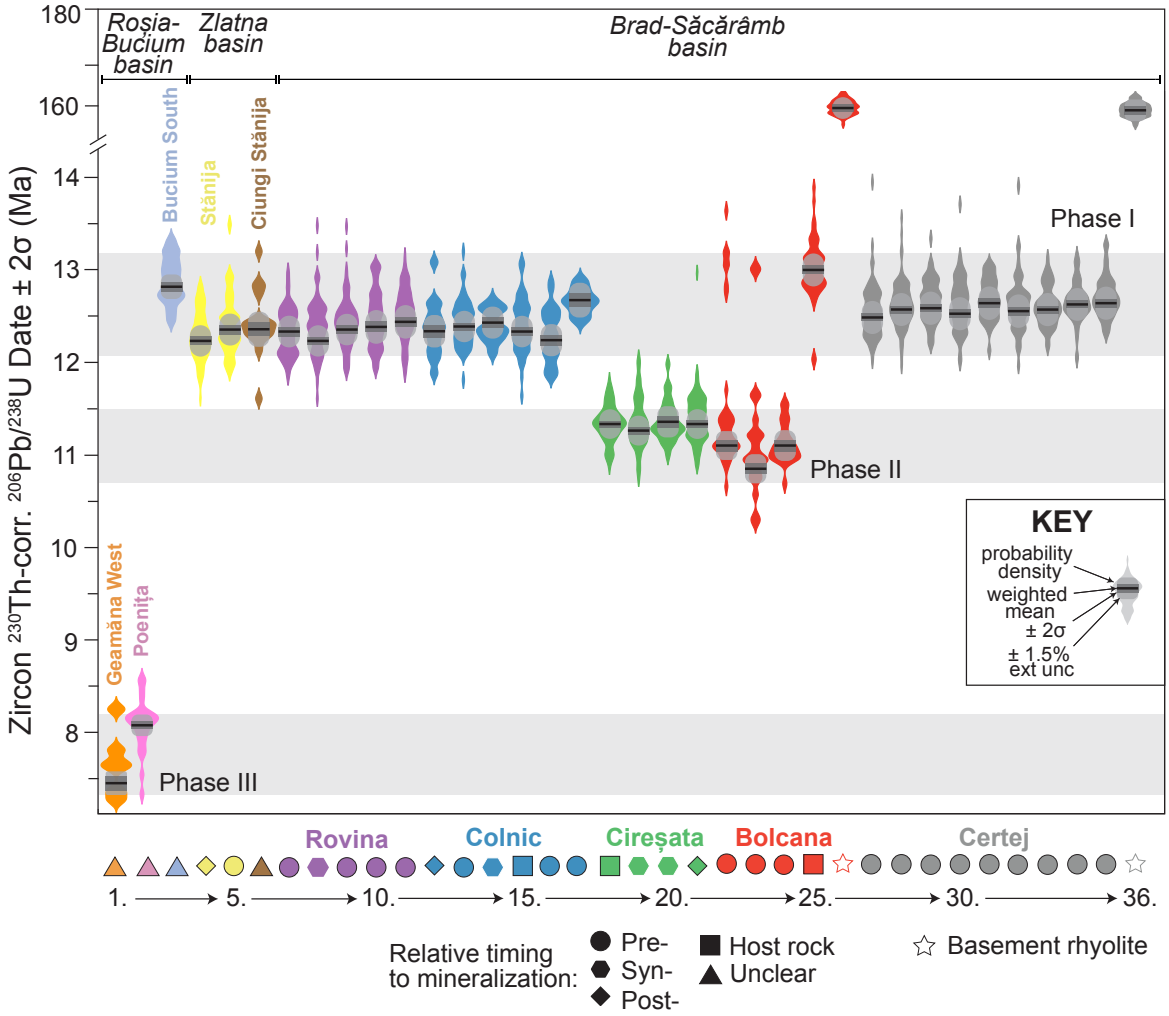

Fig. 3. Violin plot showing the probability density functions of individual ^{230}Th-corrected ^{206}Pb/^{238}U in situ zircon dates and weighted mean sample dates calculated for the intrusions in the Golden Quadrilateral. The weighted mean dates define three phases of Neogene ore-forming magmatism in the studied deposits: between 13.6 and 12.8 Ma, 12.7 and 12.5 Ma, and 9.4 and 7.2 Ma. Sample ordering from left to right follows the top-to-bottom ordering in Table 2. ext unc = external uncertainty.

dates of the relatively oldest host-rock porphyry are equivalent to those of the late post-ore dikes. One exception is the Au-Cu deposit Bolcana, in which the oldest host-rock intrusion yields a date at 13.0 ± 0.06|0.20 Ma (where the slash separates internal|external uncertainties), whereas the ore-related but premineralization porphyries yield younger dates between ~11.1 and 10.8 Ma. Two samples of the basement rhyolites from Bolcana and Certej yield weighted mean dates at 158.63 ± 0.66|2.47 and 156.74 ± 0.60|2.43 Ma, respectively.

Several samples from the deposits in the Zlatna and Brad-Săcărâmb basin contain a zircon population between ~14 and 13 Ma, which overlaps with individual zircon dates from the Bucium South porphyry and host-rock intrusion at Bolcana (Fig. 3). Also, older concordant zircon analyses from the Geamăna West intrusion at ~8.25 Ma overlap with the main population of zircon dates from the Poenița intrusion. Older concordant zircon analyses (n = 56) identified in the Neogene intrusions cover a range of ages from the Mesoarchean to Cenozoic (App. Fig. A2A), with most analyses spanning the Neoproterozoic, Permian-Triassic, and Late Cretaceous-Oligocene. Notably, no concordant zircon dates were recorded within the age range of 2.1 to 1 Ga.

Zircon trace element geochemistry

In situ zircon trace element compositions are reported in Appendix Table A4. Zircon Eu_N/Eu_N^*, ΔFMQ_{zircon}, and Ti-in-zircon crystallization temperatures for various deposits in the Golden Quadrilateral are compared in Figure 4.

The Eu_N/Eu_N^* ratios of Neogene zircon vary significantly across the individual deposits (Fig. 4A). The lowest values, mostly in the range of 0.2 to 0.4 (median values of 0.29, 0.31, and 0.34, respectively) are observed in the Au-Cu porphyry deposits Colnic, Stănija, and Ciungi Stănija. Conversely, the youngest dated zircons in the Golden Quadrilateral, from the trachyandesite intrusions at Poenița and Geamăna West, as well as intrusions at Certej, display the highest Eu_N/Eu_N^*, with median values of 0.59, 0.79, and 0.62, respectively. Zircons

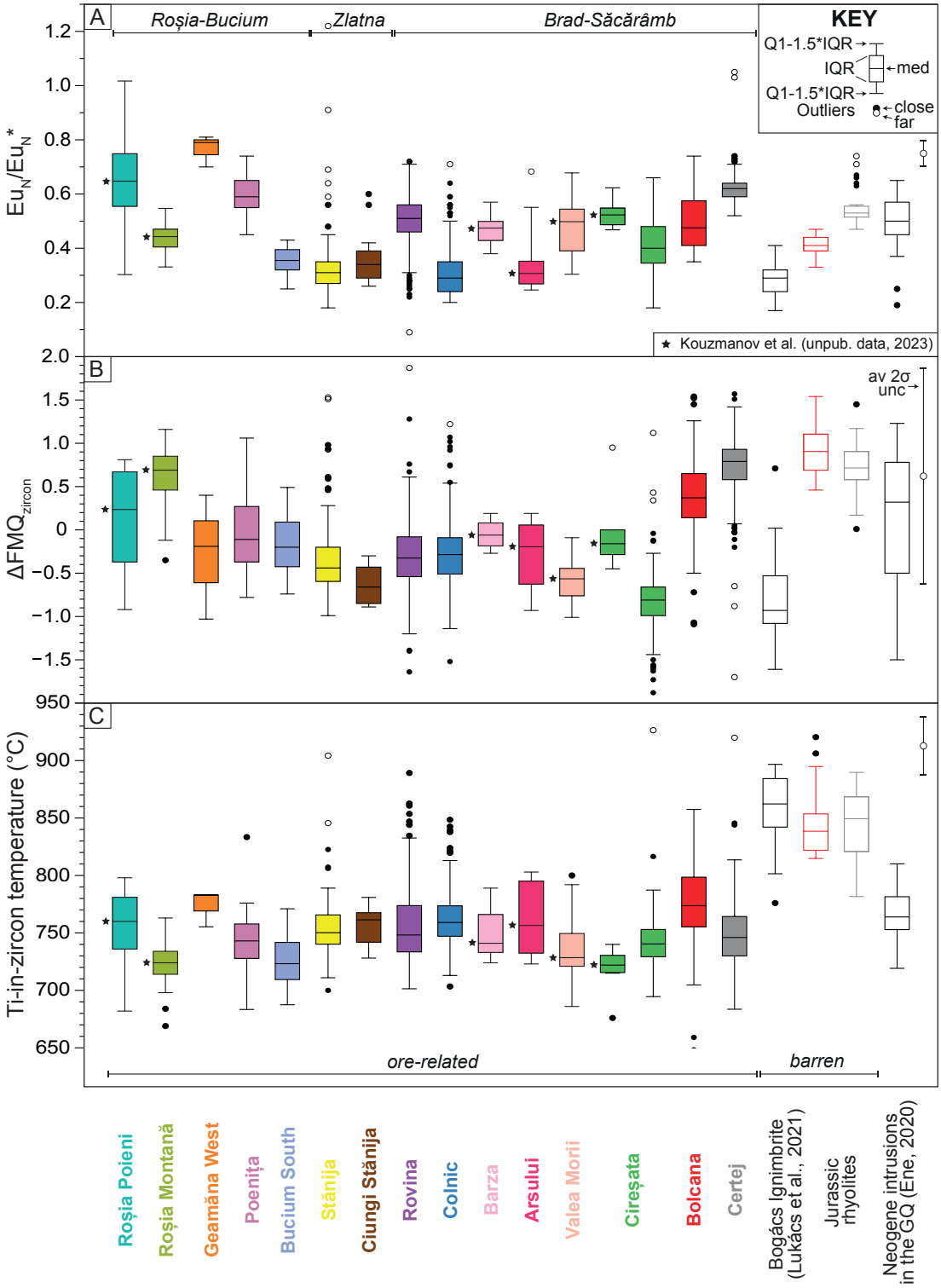

Fig. 4. Box and whisker plot of zircon Eu_N/Eu_N^* (A), ΔFMQ_{zircon} (B), and Ti-in-zircon crystallization temperature (C) for the ore-related Neogene intrusions and barren Jurassic rhyolites in the Golden Quadrilateral. Our zircon data is compared with the data for the Neogene intrusions from the Golden Quadrilateral (GQ) by K. Kouzmanov et al. (unpub. data, 2023) and Holder (2015), and data for the Bogács ignimbrite (Pannonian basin) by Lukács et al. (2021). Zircon trace element data used to calculate Eu_N/Eu_N^* and ΔFMQ values are normalized to the values for the C1 chondrite by McDonough and Sun (1995). Ti-in-zircon crystallization temperatures were computed after the calibration of Loucks et al. (2020), with assumed pressure (P) = 200 MPa and a_{TiO_2} = 0.75 for all studied rocks, and a_{SiO_2} = 0.7 or a_{SiO_2} = 1 for quartz-free or rocks containing magmatic quartz, respectively. Average 2σ uncertainties (av 2σ unc) correspond to mean values of the uncertainties on individual measurements. IQR = interquartile range, FMQ = fayalite-magnetite-quartz buffer, Q1 = first quartile, Q3 = third quartile.

from the basement rhyolites exhibit Eu_N/Eu_N^* between 0.32 and 0.47 (median = 0.41) in Bolcana and somewhat higher Eu_N/Eu_N^*, between 0.45 and 0.90 (median = 0.56) in Certej.

Zircon ΔFMQ values also scatter considerably (Fig. 4B). Zircon from Certej exhibits the most positive values (median = 0.8) among the Neogene samples, followed by Bolcana (median = 0.4), whereas the most negative values are observed in zircon from Cireşata (median = –0.8, individual analyses at –1.4) and Ciungi Stănija (median = –0.7). The ΔFMQ values of zircon from the basement rhyolites are on average higher than those from the Neogene (trachy-)andesite and dacite intrusions, with median values of 0.9 at Bolcana and 0.7 at Certej.

Ti-in-zircon temperatures of most of the Neogene intrusions range between 690° and 780°C. Somewhat higher temperatures exceeding 800°C are recorded in zircon from Rovina, Colnic, Certej, and Bolcana. Rhyolite-hosted Jurassic zircons collectively exhibit higher temperatures than the Neogene zircons, varying between 780° and 890°C and 815° and 890°C at Certej and Bolcana, respectively.

High-precision (ID-TIMS) zircon geochronology

High-precision U-Pb dates of single zircon crystals are reported with their 2σ uncertainties in Appendix Table A5 and depicted in Figure 5.

The ^{230}Th-corrected $^{206}Pb/^{238}U$ dates from the porphyry deposit Rovina range between 12.630 ± 0.016 and 12.526 ± 0.021 Ma (Fig. 5A). The dates obtained for the premineralization so-called Glam breccia (polymict but sediment clast-dominated contact breccia associated with shallow porphyry emplacement) and C1 porphyry overlap entirely within uncertainty, with equivalent youngest analyses at 12.583 ± 0.030 and 12.574 ± 0.015 Ma, respectively. Younger dates, spanning from 12.539 ± 0.015 to 12.526 ± 0.021 Ma, are resolved within the synmineralization intrusive magmatic breccia. The distribution of zircon dates from Colnic extends to that of Rovina and is bracketed by the oldest date from the Colnic porphyry (premineralization) at 12.527 ± 0.011 Ma and the youngest date from the late-mineral dike (synmineralization) at 12.448 ± 0.041 Ma. Zircon dates from intrusions at Cireşata range between 11.475 ± 0.010 Ma in the early mineral porphyry and 11.432 ± 0.009 Ma in the late postmineral dike, all overlapping within uncertainty. The same is true for the intrusions in Certej, where the oldest zircon date is recorded in the premineralization Hondol-deep porphyry at 12.782 ± 0.014 Ma and the youngest in the Hondol-shallow porphyry at 12.705 ± 0.013 Ma.

Zircon Hf isotope composition

In situ zircon Hf isotope compositions also include data of zircon from the Jurassic mid-ocean ridge basalts (MORB), gabbros and island-arc granitoids, and Cretaceous arc magmatic rocks from the broader area of the Apuseni Mts. (App. Table A6; Fig. 6)

The $\varepsilon_{Hf_{(t)}}$ of Neogene zircons from different deposits in the Golden Quadrilateral varies mostly from 2 to 10. The most positive zircon $\varepsilon_{Hf_{(t)}}$ values are recorded in the Roşia-Bucium basin: for the Cetate dacite (8) and quartz andesite (4.8) at Roşia Montană, for the biotite-bearing diorite (7.7) and host diorite (5.5) at Roşia Poieni, and for the intrusions at Geamăna West (4.4) and Poenița (3.9). The most negative values are documented for the intrusions at Ciungi Stănija (–1.5) and Stănija (–0.8) in the Zlatna basin. Distinctly negative $\varepsilon_{Hf_{(t)}}$ values, between –10 and –7.4, are identified in zircon xenocrysts entrained in the trachyandesite intrusion in Geamăna West, which yielded concordant dates at ~28 Ma. The $\varepsilon_{Hf_{(t)}}$ values of cores and rims of Neogene zircon display no apparent trend.

The $\varepsilon_{Hf_{(t)}}$ values of zircon from the Mesozoic samples generally display greater scatter. The $\varepsilon_{Hf_{(t)}}$ values of zircon from the Cretaceous (~80 Ma) magmatic rocks from the southern and northern Apuseni Mts. vary between –6 and 7.8, around a median value of 1.7. Jurassic (~158 Ma) MORB gabbros and island-arc granitoids systematically exhibit more positive zircon $\varepsilon_{Hf_{(t)}}$, with median values of 9.6 and 7.5, respectively.

Discussion

Tectonic framework for the Neogene magmatic-hydrothermal mineralization in the Golden Quadrilateral

The U-Pb zircon ages from this study, together with those from the literature, constrain the Neogene magmatic activity in the Golden Quadrilateral to an ~6.5 m.y. period between 13.61 ± 0.07 and 7.24 ± 0.04 Ma (Kouzmanov et al., 2005, 2007; Rocha, 2013; Gallhofer et al., 2015; Holder, 2015; Brunner, 2018; Müller, 2018; Ene, 2020). Each basin contains clusters of intrusions within small areas that have overall similar ages (small, <<1-m.y. variation in single-crystal ID-TIMS ages and overlapping less precise LA-ICP-MS ages; Figs. 1, 7; App. Table A7). On the other hand, among different small areas, the intrusions may differ significantly in age, indicating that brief events of magma emplacement jumped, apparently at random, between the basins and between small areas within the same basin (e.g., Roşia Montană, and Roşia Poieni in the Roşia-Bucium basin; Rovina, Colnic, Brad, Cireşata, and Valea Morii in the Brad-Barza area of the Brad-Săcărâmb basin; Certej, Bolcana, and Săcărâmb further to the southeast in the same basin; Figs. 1, 7). The small age range of intrusions in each deposit and of individual zircon in any one intrusion sample (Fig. 5) is interpreted to indicate small, short pulses of magma generation in the Golden Quadrilateral, consistent with the heterogeneous zircon and whole-rock isotopic composition and only sporadic occurrence of alkaline and adakite-like magmas. This contrasts the long-lived, presumably lower-crustal fractionation of large magma volumes characterizing giant porphyry Cu ± Au ore camps such as Tampakan (Rohrlach et al., 2005; Parra-Avila et al., 2022), El Salvador (Lee et al., 2017), Kadjaran (Rezeau et al., 2016, 2019), or Rio Blanco-Los Bronces (Large et al., 2024) and Quellaveco (Nathwani et al., 2021).

In Figure 8, we plot paleomagnetic declination against new U-Pb zircon ages for a subset of Neogene intrusions in the wider area of the Golden Quadrilateral along with previous K-Ar results, which despite analytical uncertainties show a striking correlation between age and rotation (Roşu et al, 2004a). The intrusions emplaced prior to ~12 Ma experienced larger-scale clockwise rotation (up to 70°), whereas the younger intrusions generally record only minor rotation (±~30°). Precise and accurate zircon ages largely support the older Ar dating and confirm that the Neogene intrusions in the broader Apuseni Mts. and north in the Maramureş Mts. were emplaced during large-scale clockwise rotations of the Tisza-Dacia megablock

into the Carpathian embayment (Pătrașcu et al., 1994; Panaiotu 1998, 1999; Roșu et al, 2004a). Higher positive values in older intrusions may reflect early block rotation facilitated by the retreat of the Carpathian slab, which regionally resulted in opening of detachments and steep normal faults in the neighboring Pannonian basin and shearing along major strike-slip faults throughout the Carpathian region (e.g., Tischler et al., 2007; Ustaszewski et al., 2008; Matenco and Radivojević, 2012). The formation of ore deposits in the Golden Quadrilateral does not seem preferentially related to any particular period of block rotation.

The Neogene intrusions within the Brad-Săcărâmb basin (~12.9–9.7 Ma) tend to become progressively younger in a northwest to southeast direction (Figs. 1, 7). This younging trend may reflect gradual, "zipper-like" basin opening propagating from northwest to southeast, in continuation of the

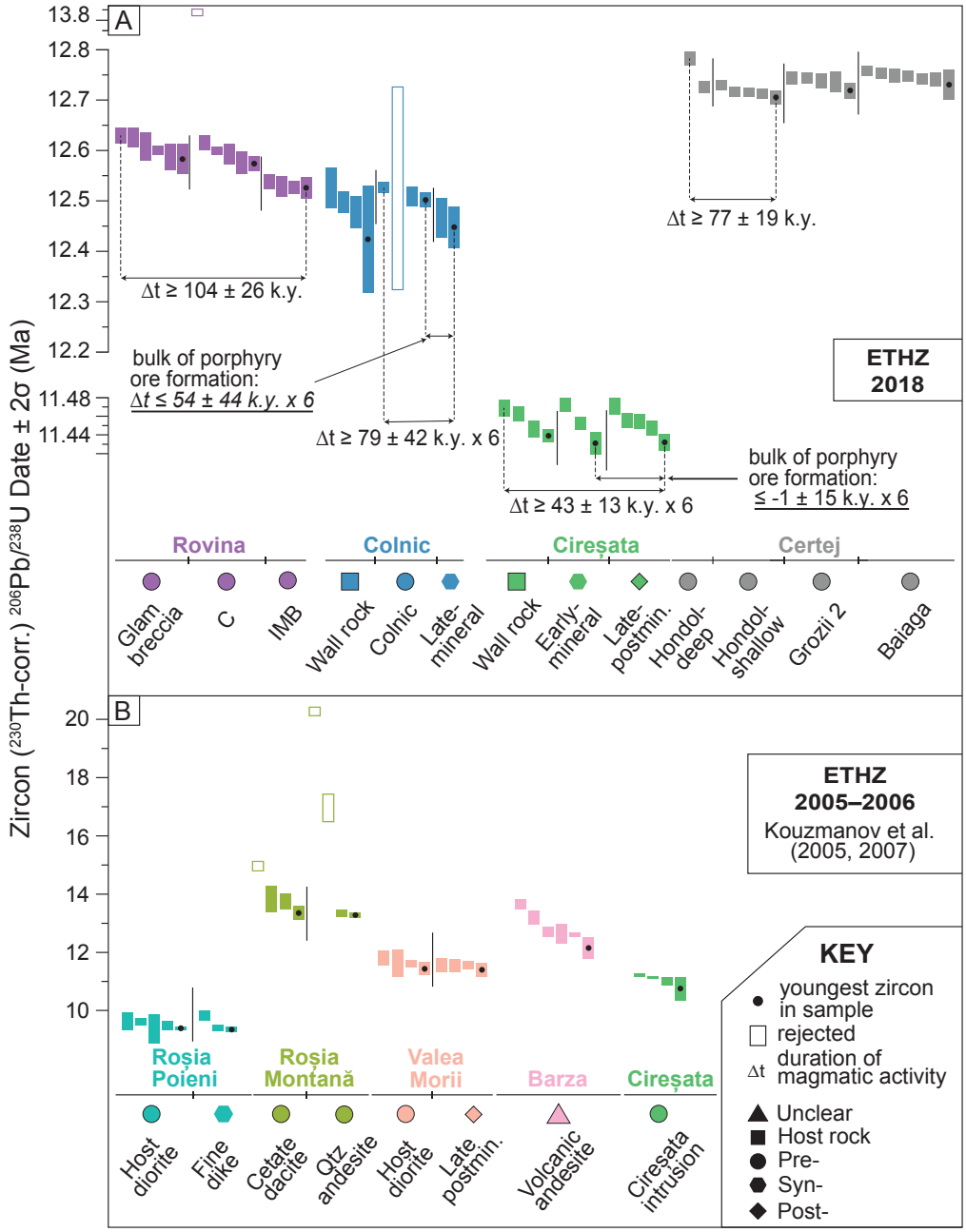

Fig. 5. High-precision ^{206}Pb/^{238}U dates of zircon from selected ore-related intrusions in the Golden Quadrilateral. A) Zircon dates for the porphyry deposits Rovina, Colnic, and Cireşata, and the epithermal deposit Certej, collected in the isotope dilution-thermal ionization mass spectrometry (ID-TIMS) U-Pb geochronology laboratory of ETH Zurich in 2018. B) Older zircon dates for the intrusions at Roșia Poieni, Roșia Montană, Valea Morii, Barza, and Cireşata, collected at ETH Zurich between 2005 and 2006 (Kouzmanov et al., 2005, 2007). Individual U-Pb zircon dates are reported with their respective 2σ uncertainties shown by error bars. Indicated timescales are calculated by subtraction, and associated uncertainties by quadratic addition of the uncertainties on individual dates. IMB = intrusive magmatic breccia, Qtz = quartz, Th-corr. = Th-corrected.

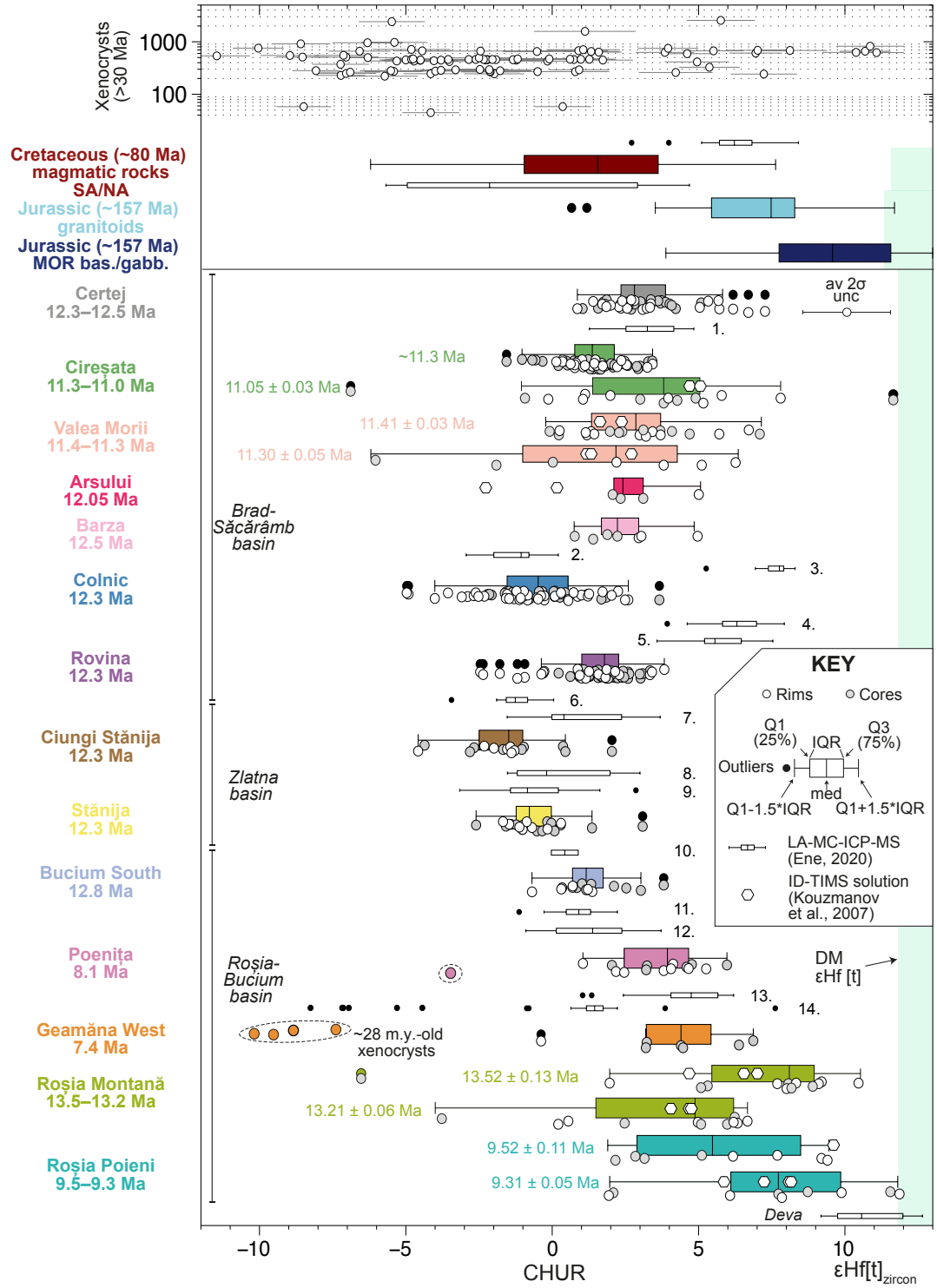

Fig. 6. Hafnium isotope composition of juvenile Neogene zircon, zircon xenocrysts, and zircon from Mesozoic magmatic rocks from the southern and northern Apuseni Mts. The $\varepsilon_{Hf[t]}$ of the depleted mantle reservoir is computed according to the model of Naeraa et al. (2012). Multiple magmatic phases at Cireşata, Valea Morii, Roşia Montană, and Roşia Poieni, as well as single magmatic phases in Arsului and Barza, are based on interpreted intrusion ages by Kouzmanov et al. (2005, 2007). Xenocryst data is from this study and Ene (2020). Intrusions from Ene (2020; see Fig. 1 for sample locations): 1 = Câinenii Mari, 2 = Dealu Fetii, 3 = Coasta Mare, 4 = Haitău, 5 = Ledişoiu, 6 = Trâmpoiele, 7 = Măgura Lupului, 8 = Almaşu Mare, 9 = Stănija, 10 = Detunata, 11 = Dealul-Conţu, 12 = Poienile-Stalnisoara, 13 = Geamăna East, 14 = Geamăna West. Abbreviations: bas = basalt, CHUR = chondritic uniform reservoir, DM = depleted mantle reservoir, gabb. = gabbro, ID-TIMS = isotope dilution-thermal ionization mass spectrometry, IQR = interquartile range, LA-MC-ICP-MS = laser ablation-multicollector-inductively coupled plasma-mass spectrometry, MOR = mid-ocean ridge, NA = North Apuseni, Q1 = first quartile, Q3 = third quartile, SA = South Apuseni, unc = uncertainty. Average 2σ uncertainty represents mean value of the uncertainties on individual measurements.

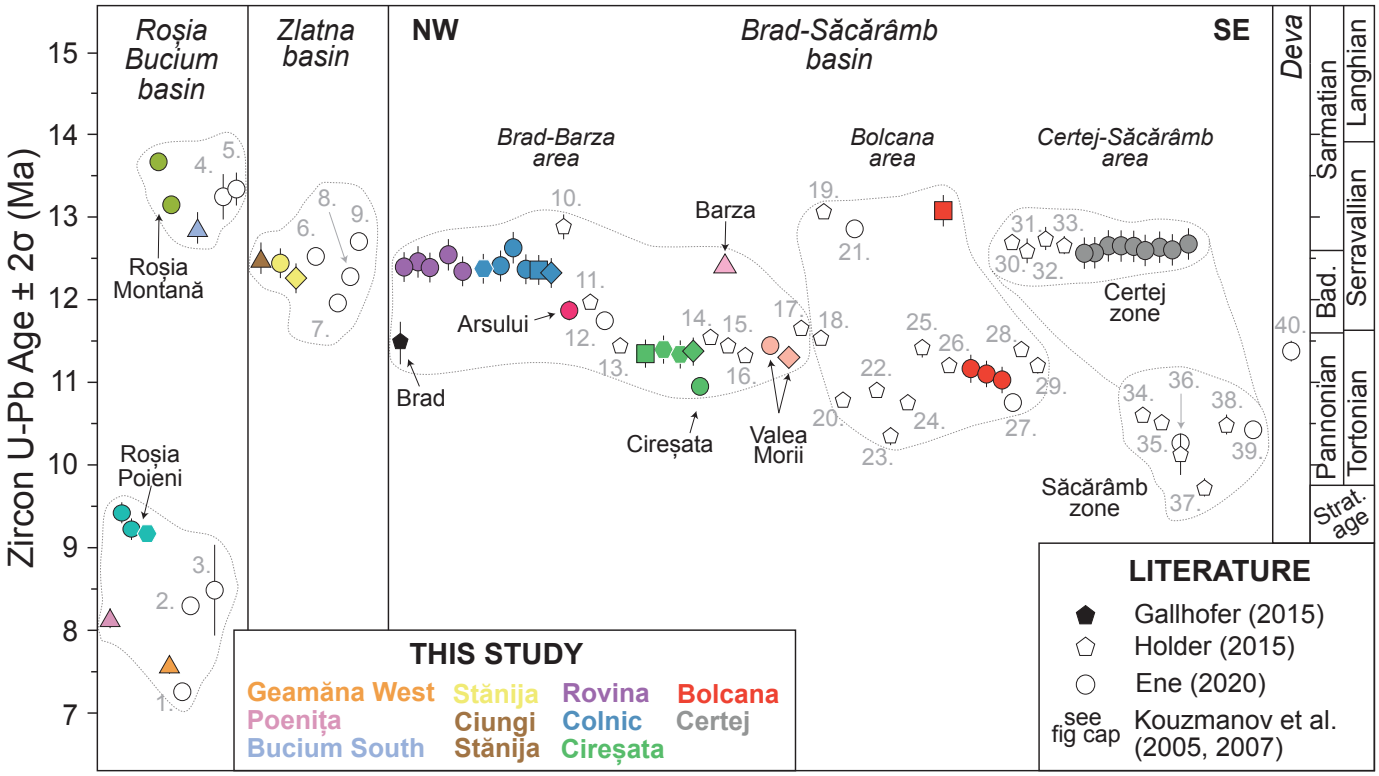

Fig. 7. Compilation of available zircon U-Pb ages for the Neogene intrusions in the Golden Quadrilateral (for sample locations, refer to Fig. 1). The ages from the Brad-Săcărâmb basin are organized from left to right along a north-northwest to south-southeast trend, and within individual deposits in random order. Ages from this study are ^{230}Th corrected and are reported with their external uncertainties, whereas the literature data are reported in their original form. Ages with no associated error bars have reported uncertainties smaller than the age symbol. Plotted ages for Roșia Montană, Roșia Poieni, Arsului, the annotated intrusion at Cireșata, as well as for Barza and Valea Morii, represent interpreted intrusion ages of Kouzmanov et al. (2005, 2007). Numbered localities in the Roșia-Bucium basin: 1 = Geamăna West, 2 = Geamăna East, 3 = Detunata, 4 = Poienile-Stalnisoara, 5 = Dealul Conțu; in the Zlatna basin: 6 = Corbu Stream/Stănija, 7 = Almașu Mare/Neagra quarry, 8 = Trâmpoiele, 9 = Măgura Lupului quarry; in the Brad-Săcărâmb basin, 10 = Valea Arsului/Arsului, 11 = Curatu, 12 = Dealul Fetii, 13 = Arisor, 14 = Cireșata, 15 = Barza Noua, 16 = Smereciu, 17 = Valea Morii, 18 = no given name in literature, 19 = Câinel, 20 = Hărțăgani, 21 = Câinenii Marii, 22 = Stirba, 23 = Cetraș, 24 = Buha, 25 = Stogu, 26 = Bolcana, 27 = Coasta Mare/Hondol-Măcriș, 28 = Fairag, 29 = Fairagut, 30 = Hondol Neckul, 31 = Hondol, 32 = Baiaga, 33 = Delul Grozii, 34 = Delul Grozii Sur, 35 = Frasinata, 36 = Haitău, 37 = Sarcău, 38 = no given name in literature, 39 = Ledișoiu, 40 = Deva. Presented data are reported in Appendix Table A7.

regional Békés-Zărand graben. Small-scale extensional melting of the mantle may have been focused at the root of the growing graben structure, with magmas subsequently channeled toward the upper crust and emplaced at the hinge of the propagating structure. The observed age progression toward the hinge in the largest basin, combined with the paleomagnetic data, likely reflects local and short-lived melt formation driven by rotation-induced extension, although concurrent subduction hydration cannot be excluded as an additional driver for melting. Isotopic heterogeneity of magmas in the Golden Quadrilateral (and occurrences of alkaline and adakite-like intrusions) further supports the local melting hypothesis over district-wide crustal fractionation.

Tracing the sources of Neogene magmas in the Golden Quadrilateral

The Neogene magmas across the Golden Quadrilateral were derived from a heterogeneously metasomatized lithospheric mantle followed by differential assimilation of preexisting crust in various basin segments ($\varepsilon_{Hf_{(t)}}$ $_{zircon}$ between –2 and 10; Fig. 6). The most primitive Hf isotope compositions are identified in zircon from the adakite-like intrusion at Deva (median ε_{Hf} = 10.6; southernmost part of the Golden Quadrilateral), from calk-alkaline magmatic rocks at Roșia Montană (8 and 4.9) and Roșia Poieni (7.7 and 5.5), and from alkaline intrusions at Poenița (3.9) and Geamăna West (4.4 and 4.7; Kouzmanov et al., 2007; Ene, 2020). Except for Deva, all are located in the Roșia-Bucium basin but include the oldest as well as the youngest Neogene intrusions in the Golden Quadrilateral. Furthermore, the Cu-Au porphyry deposits Roșia Poieni and Deva and the Au-Ag epithermal deposit Roșia Montană represent the largest deposits in the district. These magmas are only marginally less primitive than the depleted mantle melts parental to Jurassic MORB gabbros (9.6) and melts producing island-arc granitoids derived from a metasomatized mantle (7.5; Bortolotti et al., 2002, 2004; Gallhofer et al., 2017). We interpret the alkaline magmas at Poenița and Geamăna West as rare asthenospheric melts in

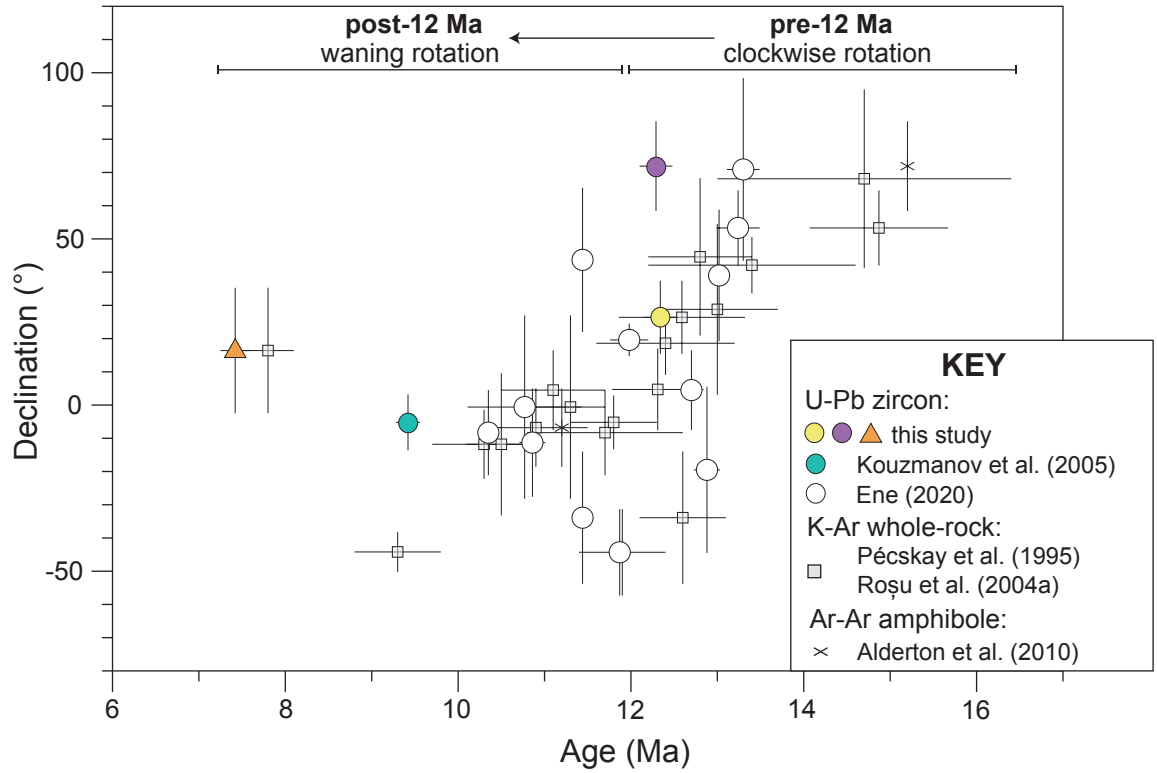

Fig. 8. Magmatic age versus palaeomagnetic declination for a subset of Neogene intrusions from the Golden Quadrilateral. Paleomagnetic data are from Pătraşcu et al. (1994), Panaiotu (1999), and Roşu et al. (2004a) and are reported in Appendix Table A8.

the Golden Quadrilateral and local isotopic heterogeneities among calc-alkaline magmas to reflect variable metasomatism of their mantle source and/or minor crustal assimilation. Most of the intrusions in the Zlatna and Brad-Săcărâmb basins (with the exception of Coasta Mare, Haitău, and Ledişoiu) exhibit more evolved, crustal-like $\varepsilon_{Hf_{(t)}zircon}$ (mostly in the range between –1 and 2; Fig. 6). They partly overlap with xenocrystic zircons sampling the composition of the local basement (Ene, 2020) and with Cretaceous arc intrusions in the Apuseni Mts. (Apuseni-Banat-Timok-Srednogorie belt) that had evolved over longer residence time in the crust (Gallhofer et al., 2015).

Zircon ε_{Hf} values of Neogene intrusions are consistent with the published mantle-like whole-rock Sr-Nd-Pb and clinopyroxene $\delta^{18}O$ (5.5–5.6‰) compositions of magmatic rocks from the broader Apuseni Mts. and regionally with mantle-derived spinel-lherzolite xenoliths and asthenosphere-derived alkali basalts from the Pannonian (e.g., Downes et al., 1992; Embey-Isztin et al., 1993; Mattey et al., 1994; Dobosi et al., 1998; Seghedi et al., 2007; Harris et al., 2013). While two studies reported a progression from more evolved toward more depleted younger magmas throughout the south Apuseni Mts. (based on whole-rock K-Ar ages and Sr-Nd-Pb isotopes; Roşu et al., 2004a; Harris et al., 2013), we observe no such trend in the zircon data.

Ample interaction of the Neogene magmas in the Golden Quadrilateral with the basement in the broadest sense is attested to by zircon xenocrysts, which are most abundant in intrusions at Colnic and in the Roşia-Bucium basin (see Fig. 6; App. Fig. A2; Ene, 2020). The age spectrum of xenocrystic zircon fingerprints Neoproterozoic, Permian through to Triassic, and Cretaceous-Cenozoic crustal sources (see App. Fig. A2A, B). The Permo-Triassic population matches the age of the Apuseni basement (e.g., Dallmeyer et al., 1999; Pană et al., 2002), and the Cretaceous-Paleogene population likely reflects the presence of Apuseni-Banat-Timok-Srednogorie–related magmatic rocks and/or lower-crustal cumulates. The Triassic and Eocene-Oligocene populations fingerprint previously unrecognized crust. Cross-basin differences partly reflect locally predominant rocks, e.g., Cretaceous flysch in the Roşia-Bucium basin and Neoproterozoic-Cambrian sources in the basement of the Brad-Săcărâmb and Zlatna basins (see App. Fig. A2B). The near absence of Jurassic-age xenocrysts indicates that the exposed Jurassic ophiolites (Brad-Săcărâmb and Zlatna basins) are restricted to the upper crust above the level of significant assimilation by the Neogene magmas.

The age spectrum of zircon xenocrysts from the Golden Quadrilateral does not resemble the detrital record of the Dacia megablock in the Inner Carpathians, on which the Golden Quadrilateral rests, but rather matches the more distant Dobrogea and Moesia blocks and partly the Dacian basement of the South Carpathians (External Carpathians; see App. Fig. A2C, D, and references therein). Diagnostic features include pronounced Neoproterozoic and Permian-Triassic peaks but rare mid-Ordovician zircon xenocrysts (e.g., Balintoni et al., 2010b, 2011a, b; Balintoni and Balica, 2016; Ducea et al., 2018; Roban et al., 2023).

Several studies proposed melting of the lower crust rather than the mantle as the dominant source for the Neogene magmas in the Golden Quadrilateral. This hypothesis was based on findings of rare andesite-hosted xenocrystic garnets in the Golden Quadrilateral that resemble garnets in granulite xenoliths in Pannonian alkali basalts (Seghedi et al., 2007). More recently, Ene (2020) argued that the enrichment in the fluid-immobile element Th in some Neogene intrusions is inconsistent with a metasomatized mantle source and that the composition of the Neogene magmas may be produced by up to 90% extension-driven melting of lower-crustal mafic cumulates. Nonetheless, this interpretation has not yet been tested against thermal constraints (cf. Heinonen et al., 2022; Storck et al., 2021; Chang and Audetat, 2023).

Utility of zircon trace element signatures as tools for exploration in the Golden Quadrilateral

Low Eu_N/Eu_N^* anomalies in zircon as indicator of high magmatic H_2O and high Ce anomalies as proxies for high magmatic oxygen fugacity have been proposed to discriminate fertile (i.e., ore-forming) from barren intrusions and magmatic districts (e.g., Ballard et al., 2002; Burnham and Berry, 2012; Trail et al., 2012; Dilles et al., 2015; Lu et al., 2016, 2017; Lee et al., 2017, 2021; Loucks et al., 2020). Figure 4 and Appendix Figure A3 test the applicability of these indicators on our example of a porphyry-epithermal district with clear Au affinity, located in an unusual tectonic setting. Pre- and synmineralization intrusions are taken to represent fertile magma batches that exsolved ore-forming hydrothermal fluids. Host-rock and postmineralization intrusions are regarded as barren magma batches emplaced prior to and/or after ore formation.

Results show neither cross- nor intradeposit patterns that could be correlated with the Au-mineralizing events at this small scale (see Fig. 4; App. Fig. A3). Between individual deposits, zircon Eu_N/Eu_N^* values range widely, from a median value of ~0.2 in the Au-rich porphyry deposits Stănija and Colnic, to ~0.6 in the Au-Ag epithermal deposit Certej, and to even higher values in the Au porphyry prospect Geamăna West (~0.8). $Eu_N/Eu_N^*{}_{zircon}$ values of the Au-mineralizing intrusions in the Golden Quadrilateral significantly overlap with the values for the Jurassic island-arc rhyolites, which are unmineralized throughout the wider region. $Eu_N/Eu_N^*{}_{zircon}$ values of some Neogene deposits also overlap with the Pannonian Miocene Bogács ignimbrite of the same age, which might approximate an erupted compositional equivalent of the ore-forming magmas in the Golden Quadrilateral (i.e., calc-alkaline andesitic and dacitic compositions; Lukács et al., 2021).

The substantial spread in zircon ΔFMQ_{zircon} across the deposits in the Golden Quadrilateral (median values between 0.8 in Certej and –0.8 in Cireşata) suggests that the Au-rich porphyry and epithermal mineralization may be associated both with oxidized and more reduced magmas (Fig. 4B; Loucks et al., 2020). Such large cross-deposit variation is surprising, given the uniform andesitic composition of nearly all ore-related intrusions (see Fig. 2; App. Table A3), and is consistent with the interpretation of small magma batches evolving in isolation. The barren Jurassic rhyolites exhibit, on average, the highest values in the region, further illustrating the disassociation between elevated zircon ΔFMQ and mineralization potential. The lowest ΔFMQ_{zircon} (i.e., most reduced) compositions are recorded for the Bogács ignimbrite, but they plot only marginally below the values for the Au-rich porphyry deposit Cireşata. Contrary to Holder (2015), we observe no correlation of zircon Eu_N/Eu_N^* or ΔFMQ and magmatic age across the district.

Within the individual deposits, zircon Eu_N/Eu_N^* and ΔFMQ do not generally correlate with ore-productive magma batches but locally reflect evolving melt composition (see App. Fig. A3). In the Au-rich porphyry deposit of Bolcana, zircons from the barren rhyolite and host-rock dacite, among others, can be discriminated based on their Eu_N/Eu_N^* and ΔFMQ values from zircon of the fertile premineralization (shell and crowded amphibole-biotite) andesites. This comparison may suggest that, on the scale of a single deposit, barren magma batches can be distinguished from fertile ones provided there is an accompanying shift in melt composition. Yet, melt composition alone cannot explain the strongly contrasting $Eu_N/Eu_N^*{}_{zircon}$ and ΔFMQ of otherwise compositionally similar andesitic intrusions in Cireşata and Certej. This suggests that additional factors, such as timing of zircon saturation, as well as abundance of other cocrystallizing REE-bearing phases (e.g., titanite, apatite, monazite, hornblende) also play an important role (e.g., Buret et al., 2016; Loader et al., 2017, 2022). In summary, zircon Eu_N/Eu_N^* and ΔFMQ do not seem diagnostic for Au-mineralizing magma pulses.

Ti-in-zircon crystallization temperatures

Zircons from the ore-related Neogene intrusions in the Golden Quadrilateral record relatively low temperatures between 690° and 780°C, with no pronounced cross-deposit differences (Fig. 4C; App. Fig. A4). Similar and even lower temperatures were reported for the giant ore Cu porphyry systems in the Andes, such as El Salvador (Chile) and Quellaveco (Peru), and at Yerington (Nevada; Dilles et al., 2015; Nathwani et al., 2021), whereas higher temperatures are recorded in barren volcanic rocks of the Apuseni area (Jurassic rhyolites at Certej, 780°–890°C, and Bolcana, 815°–890°C, and the regional Bogács ignimbrite, 800°–896°C; Lukács et al., 2021). These differences may reflect zircon saturation in relatively cool but H_2O-rich magmas giving rise to ore formation. Decreasing Ti-in-zircon temperatures with time in Roşia Poieni (from median 767° to 739°C), Roşia Montană (732°–720°C) and Stănija (761°–748°C) magmatic centers are consistent with increasing H_2O content from premineral to syn- and postmineral magmatic phases.

Lifetime of magmatic centers and duration of magmatic-hydrothermal ore formation

The total spread of zircon high-precision ages in a mineralized magmatic center indicates the minimum lifetime of magmas exposed in a composite intrusion (Schaltegger et al., 2009), whereas the youngest zircons in single intrusions that pre- and postdate hydrothermal veining and ore formation bracket the maximum duration of ore-forming hydrothermal activity (von Quadt et al., 2011). These two timescales relating to an individual magmatic-hydrothermal ore deposit are both shorter than the duration of magmatism on the scale of an entire mineral province. The latter relates to tectonic processes generating magmas in the mantle and lower crust and is also thought

to precondition the thermal state of the upper crust in the lead-up to generating an ore-forming magmatic-hydrothermal system (e.g., Lee et al., 2017; Large et al., 2021).

The youngest ID-TIMS dates constrain the emplacement age of individual intrusions (e.g., Schaltegger et al., 2009; von Quadt et al., 2011; Large et al., 2020). The Au-rich magmatic-hydrothermal systems in Rovina, Colnic, Cireşata, Bolcana, and Certej evolved over brief timescales of tens of thousands of years to a few hundred thousand years (Fig. 5A; App. Table A5). The magmatic activity associated with the Au-Cu porphyry mineralization at Rovina lasted for a minimum of ~104 ± 26 k.y., as bracketed by the oldest zircon (12.630 ± 0.016 Ma) in the premineralization Glam breccia and the youngest zircon (12.526 ± 0.021 Ma) in the premineralization intrusive breccia (intrusive magmatic breccia). At Colnic, zircon crystallization is recorded over 79 ± 42 k.y., from the age of the oldest zircon from the Colnic porphyry (12.527 ± 0.011 Ma; premineralization) to the youngest zircon from the late-mineral dike (12.448 ± 0.041 Ma; synmineralization). The youngest zircons in the Colnic porphyry (12.502 ± 0.015 Ma) and in the late-mineral dike at Colnic (12.448 ± 0.041 Ma) constrain the maximum duration of hydrothermal mineralization to 54 ± 44 k.y. (Fig. 5). High-precision ages from the Au-Cu porphyry deposit Colnic lie in perfect continuity with the ones from Rovina, suggesting that zircons from both deposits might have crystallized in sequence from a common magmatic system. However, this assumption is not supported by the distinctly lower Eu/Eu* in zircons from Colnic (0.2–0.35 compared to 0.45–0.6) and their, on average, more mantle-like Hf isotope signatures (see Figs. 4A, 6). The ore-forming magmatic activity in Cireşata lasted as short as 43 ± 13 k.y., within which all porphyry phases—from the barren wall-rock porphyry (host rock) to the late postmineral dike—were emplaced almost synchronously, as shown by overlapping ranges of high-precision zircon ages. Hydrothermal ore formation in Cireşata is bracketed by the youngest zircons of the early-mineral intrusion (11.431 ± 0.012 Ma) and postmineral dike (11.432 ± 0.009 Ma) to timescales shorter than 15 k.y. At Certej, the oldest (12.782 ± 0.014 Ma) and youngest (12.705 ± 0.013 Ma) zircon ages from the premineralization Hondol-deep and Hondol-shallow porphyry, respectively, record 77 ± 19 k.y. of magmatic zircon crystallization, but the age and duration of subsequent ore deposition are not further constrained.

The Au-dominated mineral province Golden Quadrilateral records a 6.5-m.y.-long duration of calc-alkaline magmatism but much shorter duration of magmatic-hydrothermal activity in each deposit, constrained to less than ~100 k.y. These two timescales are similar to other Cu ± Au mineral provinces containing small to midsized porphyry deposits worldwide (e.g., Halter et al., 2004; Chelle-Michou et al., 2014, 2015; Buret et al., 2016; Tapster et al., 2016; Large et al., 2018). What may be peculiar in the Golden Quadrilateral is that the minimum duration of magmatic zircon crystallization in each mineralized center, including distinctly pre-ore host intrusions and volcanic rocks, is unusually brief compared to these published examples. This is consistent with the interpretation that the magma reservoirs eventually saturating ore-forming hydrothermal fluids are small and cool rapidly in the upper crust. Geochronological constraints do not exclude that the magmas were prepared over longer periods at greater depth, as suggested by variably adakitic magma compositions, but the observed differences in geochemical characteristics of closely neighboring magmatic centers of similar age make a long-lived, large common reservoir in the lower crust a rather unlikely case for the Golden Quadrilateral.

Conclusions

Zircon petrochronology and rock geochemistry that were used to investigate the time-space patterns, sources, composition, and duration of the Neogene calc-alkaline magmatism associated with the Au-rich porphyry and epithermal mineralization in the Golden Quadrilateral (Apuseni Mts., Romania) led to the following findings:

1. New and published U-Pb zircon ages show that the ore-related magmatism in the Golden Quadrilateral took place almost continuously between 13.61 ± 0.07 (Roşia Montană) and 7.24 ± 0.04 Ma (Geamăna West) but in brief events jumping in time between different segments of three extensional basins. The U-Pb ages confirm a correlation of intrusion age with paleomagnetic declination at the scale of the entire ore district, indicating magma emplacement synchronous with rotation-induced extension in a southwest-northeast direction. The magmatism in the Golden Quadrilateral evolved during the rotation of the Tisza-Dacia megablock, which triggered the opening of the basins in the Golden Quadrilateral and partial melting of the subjacent mantle and provided pathways for the ore-forming magmas to the upper crust. Within the largest basin (Brad-Săcărămb), a SE-directed younging trend in magmatic ages tracks the propagation of an underlying graben structure from the neighboring Pannonian basin into the Golden Quadrilateral.
2. The Neogene magmas in the Golden Quadrilateral were predominantly derived from a locally heterogeneous lithospheric mantle and incorporated various proportions of the preexisting crust ($\varepsilon_{Hf_{zircon}}$ between –2 and 10). The most mantle-like magmas in the Golden Quadrilateral are associated with the oldest and the youngest magmatic activity in the Golden Quadrilateral, and they gave rise to the three largest deposits in the region: Roşia Poieni, Roşia Montană, and Deva. Age spectra of xenocrystic zircon more closely correspond to European continental basement rather than the Dacian megablock in the Inner Carpathians, on which the Golden Quadrilateral rests today.
3. Europium anomaly (Eu_N/Eu_N^*) and ΔFMQ of zircon, commonly used as fertility indicators for porphyry Cu systems, reveal no systematic patterns with respect to the ore-forming events in the Golden Quadrilateral. High and low Eu_N/Eu_N^* and ΔFMQ_{zircon} values derived from zircon trace element concentrations imply that the Au-rich porphyry and epithermal mineralization in the Golden Quadrilateral is not systematically associated with unusually H_2O-rich or oxidized magmas.
4. The maximum duration of magmatic-hydrothermal activity in individual deposits in the Golden Quadrilateral is bracketed by high-precision (ID-TIMS) U-Pb zircon geochronology to below 100 k.y. This finding, together with small-scale trace element variations, indicates separate magmatic fluid sources of small to moderate dimensions.

Acknowledgments

The authors wish to thank Paul Ivăşcanu, Tim Baker, Călin Tămaş, Zsolt Kulcsár, Réka Dénes, Randy Ruff, Sorin Halga, and Tim Fletcher for their guidance during field work and sampling in the Golden Quadrilateral and for sharing with us the unpublished mine geologic data and their knowledge of local geology. We further thank the teams of Eldorado Gold, Barrick Gold, Carpathian Gold (Euro Sun Mining), and Deva Gold for granting access to the exploration sites and for their logistical support. We extend our gratitude to Vivian Santana Rocha for acquiring the preliminary in situ zircon U-Pb and trace element data, Stefan M. Schmid for reading an early version of the manuscript, Remy Lüchinger and Lydia Zehnder for their help with sample preparation, and David Holder for sharing his data set with us. Field work in the Golden Quadrilateral (Romania) conducted by S.M., M.B., and L.M. was partly funded by the Grubenmann-Burri travel grant of ETH Zurich. Finally, S.M. acknowledges the generous financial support of ETH Zurich (ERDW scholarship) received for the duration of his M.Sc. studies.

REFERENCES

AGP Mining Consultants Inc., 2012, NI 43-101 Technical Report on the Rovina Valley Project, West-Central Romania (Mineral Resource Estimate Update): Technical Report for Carpathian Gold Inc., August 30, 2012.

——2019, NI 43-101 Technical Report on the Rovina Valley Project in Romania, Preliminary Economic Assessment: Technical Report for Euro Sun Mining Inc., February 20, 2019.

Alderton, D., Pécskay, Z., and Snee, L., 2010, The timing of volcanism and associated precious metal mineralization in the Apuseni Mountains, Romania: Scientific Annual of the Department of Geology, v. 39, p. 22.

Alexander, R., Juras, S., Miller, R., and Kalanchey, R., 2014, Technical report for the Certej project: Romania, Eldorado Gold, 190 p., https://www.miningdataonline.com/reports/Certej_Technical_Report_Feb_2014.pdf.

Apopei, A.I., Buzgar, N., Damian, G., and Buzatu, A., 2014a, The Raman study of the weathering minerals from the Coranda-Hondol open pit (Certej gold-silver deposit) and their photochemical degradation products under laser irradiation: The Canadian Mineralogist, v. 52, p. 1027–1038.

Apopei, A.I., Damian, G., Buzgar, N., Milovska, S., and Buzatu, A., 2014b, New occurrences of hessite, petzite and stützite at Coranda-Hondol open pit (Certej gold-silver deposit, Romania): Carpathian Journal of Earth and Environmental Sciences, v. 9, p. 71–78.

Apopei, A.I., Damian, G., Buzgar, N., and Buzatu, A., 2016, Mineralogy and geochemistry of Pb-Sb/As-sulfosalts from Coranda-Hondol ore deposit (Romania)—conditions of telluride deposition: Ore Geology Reviews, v. 72, p. 857–873.

Baker, T., 2019, Gold ± copper endowment and deposit diversity in the Western Tethyan magmatic belt, southeast Europe: Implications for exploration: Economic Geology, v. 114, p. 1237–1250.

Bala, A., Toma-Danila, D., Tataru, D., and Grecu, B., 2017, Crustal models assessment in western part of Romania employing active seismic and seismologic methods: IOP Conference Series: Earth and Environmental Science, v. 95, article 032026.

Balintoni, I., and Balica, C., 2016, Peri-Amazonian provenance of the Euxinic craton components in Dobrogea and of the North Dobrogean orogen components (Romania): A detrital zircon study: Precambrian Research, v. 278, p. 34–51.

Balintoni, I., Balica, C., Cliveţi, M., Li, L.Q., Hann, H.P., Chen, F.K., and Schuller, V., 2009, The emplacement age of the Muntele Mare Variscan granite (Apuseni Mountains, Romania): Geologica Carpathica, v. 60, p. 495–504.

Balintoni, I., Balica, C., Ducea, M.N., Hann, H.P., and Şabliovschi, V., 2010a, The anatomy of a Gondwanan terrane: The Neoproterozoic-Ordovician basement of the pre-Alpine Sebeş-Lotru composite terrane (South Carpathians, Romania): Gondwana Research, v. 17, p. 561–572.

Balintoni, I., Balica, C., Ducea, M.N., Zaharia, L., Chen, F.K., Cliveţi, M., Hann, H.P., Li, L.Q., and Ghergari, L., 2010b, Late Cambrian-Ordovician northeastern Gondwanan terranes in the basement of the Apuseni Mountains, Romania: Journal of the Geological Society, London, v. 167, p. 1131–1145.

Balintoni, I., Balica, C., Seghedi, A., and Ducea, M.N., 2010c, Avalonian and Cadomian terranes in north Dobrogea, Romania: Precambrian Research, v. 182, p. 217–229.

Balintoni, I., Balica, C., Seghedi, A., and Ducea, M., 2011a, Peri-Amazonian provenance of the Central Dobrogea terrane (Romania) attested by U/Pb detrital zircon age patterns: Geologica Carpathica, v. 62, p. 299–307.

Balintoni, I., Balica, C., Ducea, M.N., and Stremţan, C., 2011b, Peri-Amazonian, Avalonian-type and Ganderian-type terranes in the South Carpathians, Romania: The Danubian domain basement: Gondwana Research, v. 19, p. 945–957.

Balintoni, I., Balica, C., Ducea, M.N., and Hann, H.P., 2014, Peri-Gondwanan terranes in the Romanian Carpathians: A review of their spatial distribution, origin, provenance, and evolution: Geoscience Frontiers, v. 5, p. 395–411.

Ballard, J.R., Palin, M.J., and Campbell, I.H., 2002, Relative oxidation states of magmas inferred from Ce (IV)/Ce (III) in zircon: Application to porphyry copper deposits of northern Chile: Contributions to Mineralogy and Petrology, v. 144, p. 347–364.

Berza, T., Constantinescu, E., and Vlad, S.N., 1998, Upper Cretaceous magmatic series and associated mineralisation in the Carpathian-Balkan orogen: Resource Geology, v. 48, p. 291–306.

Blannin, R., Frenzel, M., Tusa, L., Birtel, S., Ivăşcanu, P., Baker, T., and Gutzmer, J., 2021, Uncertainties in quantitative mineralogical studies using scanning electron microscope-based image analysis: Minerals Engineering, v. 167, article 106836.

Bortolotti, V., Marroni, M., Nicolae, I., Pandolfi, L., Principi, G., and Saccani, E., 2002, Geodynamic implications of Jurassic ophiolites associated with island-arc volcanics, South Apuseni Mountains, western Romania: International Geology Review, v. 44, p. 938–955.

Bortolotti, V., Marroni, M., Nicolae, I., Pandolfi, L., Principi, G., and Saccani, E., 2004, An update of the Jurassic ophiolites and associated calc-alkaline rocks in the South Apuseni Mountains (western Romania): Ofioliti, v. 29, p. 5–18.

Bouvier, A., Vervoort, J.D., and Patchett, P.J., 2008, The Lu-Hf and Sm-Nd isotopic composition of CHUR: Constraints from unequilibrated chondrites and implications for the bulk composition of terrestrial planets: Earth and Planetary Science Letters, v. 273, p. 48–57.

Bowring, J.F., McLean, N.M., and Bowring, S.A., 2011, Engineering cyber infrastructure for U-Pb geochronology: Tripoli and U-Pb_Redux: Geochemistry Geophysics Geosystems, v. 12, p. 1–19.

Brunner, M., 2018, U/Pb zircon dating of Miocene magmatism in the Apuseni Mountains (Romania) and time relationship of intrusive events at the Certej deposit: M.Sc. thesis, Zurich, Switzerland, ETH Zurich, 73 p.

Buret, Y., von Quadt, A., Heinrich, C., Selby, D., Wälle, M., and Peytcheva, I., 2016, From a long-lived upper-crustal magma chamber to rapid porphyry copper-emplacement: Reading the geochemistry of zircon crystals at Bajo de la Alumbrera (NW Argentina): Earth and Planetary Science Letters, v. 450, p. 120–131.

Buret, Y., Wotzlaw, J.F., Roozen, S., Guillong, M., von Quadt, A., and Heinrich, C.A., 2017, Zircon petrochronological evidence for a plutonic-volcanic connection in porphyry copper deposits: Geology, v. 45, p. 623–626.

Burnham, A.D., and Berry, A.J., 2012, An experimental study of trace element partitioning between zircon and melt as a function of oxygen fugacity: Geochimica et Cosmochimica Acta, v. 95, p. 196–212.

Cardon, O., André-Mayer, A.S., Sausse, J., Milu, V., Chauvet, A., Leroy, J.L., Lespinasse, M., and Udubasa, S., 2005, Connexion porphyre cuprifère-épithermaux de type low-sulfidation: Analyse structurale et representation 3D du secteur de Bolcana, monts Apuseni, Roumanie: Comptes Rendus Geoscience, v. 337, p. 824–831.

Cardon, O., Reisberg, L., André-Mayer, A.S., Leroy, J., Milu, V., and Zimmermann, C., 2008, Re-Os systematics of pyrite from the Bolcana porphyry copper deposit, Apuseni Mountains, Romania: Economic Geology, v. 103, p. 1695–1702.

Carminati, E., Lustrino, M., and Doglioni, C., 2012, Geodynamic evolution of the central and western Mediterranean: Tectonics vs. igneous petrology constraints: Tectonophysics, v. 579, p. 173–192.

Chang, J., and Audétat, A., 2023, Post-subduction porphyry Cu magmas in the Sanjiang region of southwestern China formed by fractionation of lithospheric mantle-derived mafic magmas: Geology, v. 51, p. 64–68.

Chelle-Michou, C., Chiaradia, M., Ovtcharova, M., Ulianov, A., and Wotzlaw, J.F., 2014, Zircon petrochronology reveals the temporal link between porphyry systems and the magmatic evolution of their hidden plutonic roots (the Eocene Coroccohuayco deposit, Peru): Lithos, v. 198, p. 129–140.

Chelle-Michou, C., Chiaradia, M., Selby, D., Ovtcharova, M., and Spikings, R.A., 2015, High-resolution geochronology of the Coroccohuayco porphyry-skarn deposit, Peru: A rapid product of the Incaic orogeny: Economic Geology, v. 110, p. 423–443.

Chelle-Michou, C., Rottier, B., Caricchi, L., and Simpson, G., 2017, Tempo of magma degassing and the genesis of porphyry copper deposits: Scientific Reports, v. 7, p. 1–12.

Chu, N.C., Taylor, R.N., Chavagnac, V., Nesbitt, RW., Boella, R.M., Milton, J.A., German, C.R., Bayon, G., and Burton, K., 2002, Hf isotope ratio analysis using multi-collector inductively coupled plasma mass spectrometry: An evaluation of isobaric interference corrections: Journal of Analytical Atomic Spectrometry, v. 17, p. 1567–1574.

Cioacă, M.E., Munteanu, M., Qi, L., and Costin, G., 2014, Trace element concentrations in porphyry copper deposits from Metaliferi Mountains, Romania: A reconnaissance study: Ore Geology Reviews, v. 63, p. 22–39.

Ciobanu, C.L., Cook, N.J., and Stein, H., 2002, Regional setting and geochronology of the Late Cretaceous Banatitic magmatic and metallogenetic belt: Mineralium Deposita, v. 37, p. 541–567.

Condon, D.J., Schoene, B., McLean, N.M., Bowring, S.A., and Parrish, R.R., 2015, Metrology and traceability of U-Pb isotope dilution geochronology (EARTHTIME tracer calibration part I): Geochimica et Cosmochimica Acta, v. 164, p. 464–480.

Cook, N.J., and Ciobanu, C.L., 2004, Au-Ag-telluride deposits of the Golden Quadrilateral, Apuseni Mts., Romania (Guidebook of the International Field Workshop of IGCP project 486): International Association on the Genesis of Ore Deposits (IAGOD) Guidebook Series, v. 12, 266 p.

Dallmeyer, R.D., Pană, D.I., Neubauer, F., and Erdmer, P., 1999, Tectonothermal evolution of the Apuseni Mountains, Romania: Resolution of Variscan versus Alpine events with $^{40}Ar/^{39}Ar$ ages: The Journal of Geology, v. 107, p. 329–352.

Dénes, R., Márton, I., Kiss, G.B., Ivăşcanu, P.M., and Veress, Z., 2014, Additional data regarding the petrography and geochemistry of the magmatic phases and hydrothermal vein types from Bolcana porphyry Cu-Au mineralization (Apuseni Mts., Romania): Romanian Journal of Mineral Deposits, v. 87, p. 99–104.

Dilles, J.H., Kent, A.J.R., Wooden, J.L., Tosdal, R.M., Koleszar, A., Lee, R.G., and Farmer, L.P., 2015, Zircon compositional evidence for sulfur-degassing from ore-forming arc magmas: Economic Geology, v. 110, p. 241–251.

Dobosi, G., Downes, H., Mattey, D., and Embey-Isztin, A., 1998, Oxygen isotope ratios of phenocrysts from alkali basalts of the Pannonian basin: Evidence for an O-isotopically homogeneous upper mantle beneath a subduction-influenced area: Lithos, v. 42, p. 213–223.

Downes, H., Embey-Isztin, A., and Thirlwall, M., 1992, Petrology and geochemistry of spinel peridotite xenoliths from the western Pannonian basin (Hungary): Evidence for an association between enrichment and texture in the upper mantle: Contributions to Mineralogy and Petrology, v. 109, p. 340–354.

Ducea, M.N., Negulescu, E., Profeta, L., Săbău, G., Jianu, D., Petrescu, L., and Hoffman, D., 2016, Evolution of the Sibişel shear zone (South Carpathians): A study of its type locality near Răşinari (Romania) and tectonic implications: Tectonics, v. 35, p. 2131–2157.

Ducea, M.N., Giosan, L., Carter, A., Balica, C., Stoica, A.M., Roban, R.D., Balintoni, I., Filip, F., and Petrescu, L., 2018, U-Pb detrital zircon geochronology of the Lower Danube and its tributaries: Implications for the geology of the Carpathians: Geochemistry, Geophysics, Geosystems, v. 19, p. 3208–3223.

Dunkl, I., Schuller, V., Frisch, W., Danišik, M., and Melinte, M.C., 2009, Upper Cretaceous Gosau deposits of the Apuseni Mountains (Romania)—similarities and differences to the Eastern Alps: Austrian Journal of Earth Sciences, v. 102, p. 133–145.

Eldorado Gold, 2020, Eldorado Gold Mineral Reserves as of September 30, 2020: www.eldoradogold.com/assets/resources-and-reserves/default.aspx, accessed July 25, 2021.

Embey-Isztin, A., Downes, H., James, D.E., Upton, B.G.J., Dobosi, G., Ingram, G.A., Harmon, R.S., and Scharbert, H.G., 1993, The petrogenesis of Pliocene alkaline volcanic rocks from the Pannonian basin, Eastern Central Europe: Journal of Petrology, v. 34, p. 317–343.

Ene, V.V., 2020, Crustal recycling in the magmatic evolution of post-subduction provinces: The South Apuseni Mountains, Romania: Ph.D. thesis, Leicester, UK, University of Leicester, 302 p.

Engi, M., Lanari, P., and Kohn, M.J., 2017, Significant ages—an introduction to petrochronology: Reviews in Mineralogy and Geochemistry, v. 83, p. 1–12.

Ferry, J.M., and Watson, E.B., 2007, New thermodynamic models and revised calibrations for the Ti-in-zircon and Zr-in-rutile thermometers: Contributions to Mineralogy and Petrology, v. 154, p. 429–437.

Fu, B., Mernagh, T.P., Kita, N.T., Kemp, A.I.S., and Valley, J.W., 2009, Distinguishing magmatic zircon from hydrothermal zircon: A case study from the Gidginbung high-sulphidation Au-Ag-(Cu) deposit, SE Australia: Chemical Geology, v. 259, p. 131–142.

Gál, A., Molnár, F., Szakács, A., Kristály, F., Weiszburg, T.G., and Pécskay, Z., 2010, The Certej hydrothermal ore deposit (Apuseni Mts., Romania): Fluid inclusions, types and age of the related hydrothermal alteration [ext. abs.]: Congress of the Carpathian-Balkan Geological Association, Thessaloniki, Greece, 2010, Extended Abstracts, v. 39, p. 118.

Gallhofer, D., von Quadt, A., Peytcheva, I., Schmid, S.M., and Heinrich, C.A., 2015, Tectonic, magmatic, and metallogenic evolution of the Late Cretaceous arc in the Carpathian-Balkan orogen: Tectonics, v. 34, p. 1813–1836.

Gallhofer, D., von Quadt, A., Schmid, S.M., Guillong, M., Peytcheva, I., and Seghedi, I., 2017, Magmatic and tectonic history of Jurassic ophiolites and associated granitoids from the South Apuseni Mountains (Romania): Swiss Journal of Geosciences, v. 110, p. 699–719.

Ghitulescu, T.P., and Socolescu, M., 1941, Etude géologique et minière des monts métallifères (quadrilatère, aurifère et régions environnantes): Anuarul Institutului Geologic Roman, v. 11, p. 181–463.

Guillong, M., Meier, D.L., Allan, M.M., Heinrich, C.A., and Yardley, B.W., 2008, Appendix A6: SILLS: A MATLAB-based program for the reduction of laser ablation ICP-MS data of homogeneous materials and inclusions: Mineralogical Association of Canada Short Course, v. 40, p. 328–333.

Halga, S., Ruff, R., Stefanini, B., and Nicolici, A., 2010, The Rovina Valley project, Apuseni Mts., Romania: Gold-copper porphyry discoveries in a historic mining district: Romanian Journal of Mineral Deposits, v. 84, p. 12–14.

Halter, W.E., Bain, N., Becker, K., Heinrich, C.A., Landtwing, M., von Quadt, A., Clark, A.H., Sasso, A.M., and Tosdal, R.M., 2004, From andesitic volcanism to the formation of a porphyry Cu-Au mineralizing magma chamber: The Farallón Negro Volcanic Complex, northwestern Argentina: Journal of Volcanology and Geothermal Research, v. 136, p. 1–30.

Harris, C.R., Pettke, T., Heinrich, C.A., Rosu, E., Woodland, S., and Fry, B., 2013, Tethyan mantle metasomatism creates subduction geochemical signatures in non-arc Cu-Au-Te mineralizing magmas, Apuseni Mountains (Romania): Earth and Planetary Science Letters, v. 366, p. 122–136.

Hedenquist, J.W., and Lowenstern, J.B., 1994, The role of magmas in the formation of hydrothermal ore-deposits: Nature, v. 370, p. 519–527.

Heinonen, J.S., Spera, F.J., and Bohrson, W.A., 2022, Thermodynamic limits for assimilation of silicate crust in primitive magmas: Geology, v. 50, p. 81–85.

Holder, D., 2015, Geological and geochemical controls for epithermal Au-Ag-Te (Pb-Zn) mineralisation at Coranda-Hondol and the Brad-Sacaramb basin mineral district of western Romania: Ph.D. thesis, London, Kingston University, 381 p.

Horstwood, M.S., Košler, J., Gehrels, G., Jackson, S.E., McLean, N.M., Paton, C., Pearson, N.J., Sircombe, K., Sylvester, P., Vermeesch, P., Bowring, J.F., Condon, D.J., and Schoene, B., 2016, Community-derived standards for LA-ICP-MS U-(Th-)Pb geochronology-uncertainty propagation, age interpretation and data reporting: Geostandards and Geoanalytical Research, v. 40, p. 311–332.

Ianovici, V., Giuşcă, D., Ghiţulescu, T.P., Borcoş, M., Lupu, M., Bleahu, M., and Savu, H., 1969, Evoluţia geologică a Munţilor Metaliferi: Bucharest, Romania, Editura Academie Republicii Socialiste România, 741 p.

Ivascanu, P.M., Pettke, T., Kouzmanov, K., Heinrich, C.A., Pintea, I., Roşu, E., and Udubasa, G., 2003, The magmatic to hydrothermal transition: Miocene Deva porphyry copper-gold deposit, South Apuseni Mts, Romania [ext. abs.]: Mineral Exploration and Sustainable Development: Society for

Geology Applied to Mineral Deposits (SGA), Biennial Meeting, 7th, Athens, Greece, 2003, Extended Abstracts, p. 24–28.

Ivascanu, P.M., Baker, T., Lewis, P., Kulcsar, Z., Denes, R., and Tamas, C., 2019, Bolcana, Romania: Geology and discovery history of a gold rich porphyry deposit [ext. abs.]: NewGenGold, Perth, Australia, 2019, Extended Abstracts, p. 69–82.

Jaffey, A.H., Flynn, K.F., Glendenin, L.E., Bentley, W.C., and Essling, A.M., 1971, Precision measurement of half-lives and specific activities of ^{235}U and ^{238}U: Physical Review C, v. 4, p. 1889–1906.

Janković, S., 1997, The Carpatho-Balkanides and adjacent area: A sector of the Tethyan Eurasian metallogenic belt: Mineralium Deposita, v. 32, p. 426–433.

Kounov, A., and Schmid, S.M., 2013, Fission-track constraints on the thermal and tectonic evolution of the Apuseni Mountains (Romania): International Journal of Earth Sciences, v. 102, p. 207–233.

Kouzmanov, K., Pettke, T., Heinrich, C.A., Riemer, S., Ivascanu, P.M., and Roşu, E., 2003, The porphyry to epithermal transition in a magmatic-hydrothermal system: Valea Morii copper-gold deposit, Apuseni Mts, Romania [ext. abs.]: Mineral Exploration and Sustainable Development: Society for Geology Applied to Mineral Deposits (SGA), Biennial Meeting, 7th, Athens, Greece, 2003, Extended Abstracts, p. 303–306.

Kouzmanov, K., von Quadt, A., Peytcheva, I., Harris, C., Heinrich, C.A., Roşu, E., and O'Connor, G., 2005, Rosia Poieni porphyry Cu-Au and Rosia Montana epithermal Au-Ag deposits, Apuseni Mts, Romania: Timing of magmatism and related mineralisation: Bulgarian Academy of Sciences, v. 43, p. 113–117.

Kouzmanov, K., von Quadt, A., Peytcheva, I., Harris, C.R., Heinrich, C.A., Roşu, E., and Ivascanu, P.M., 2007, Miocene magmatism and ore formation in the South Apuseni Mountains, Romania: New genetic and timing constraints [ext. abs.]: Digging Deeper: Society for Geology Applied to Mineral Deposits (SGA), Biennal Meeting, 9th, Dublin, Ireland, 2007, Extended Abstracts, p. 865–868.

Krezsek, C., Bercea, R.I., Tari, G., and Ionescu, G., 2018, Cretaceous sedimentation along the Romanian margin of the Black Sea: Inferences from onshore to offshore correlations: Geological Society, London, Special Publications, v. 464, p. 211–245.

Krogh, T.E., 1973, A low-contamination method for hydrothermal decomposition of zircon and extraction of U and Pb for isotopic age determinations: Geochimica et Cosmochimica Acta, v. 37, p. 485–494.

Large, S.J.E., von Quadt, A., Wotzlaw, J.F., Guillong, M., and Heinrich, C.A., 2018, Magma evolution leading to porphyry Au-Cu mineralization at the Ok Tedi deposit, Papua New Guinea: Trace element geochemistry and high-precision geochronology of igneous zircon: Economic Geology, v. 113, p. 39–61.

Large, S.J.E., Wotzlaw, J.F., Guillong, M., von Quadt, A., and Heinrich, C.A., 2020, Resolving the timescales of magmatic and hydrothermal processes associated with porphyry deposit formation using zircon U-Pb petrochronology: Geochronology, v. 2, p. 209–230.

Large, S.J.E., Buret, Y., Wotzlaw, J.F., Karakas, O., Guillong, M., von Quadt, A., and Heinrich, C.A., 2021, Copper-mineralised porphyries sample the evolution of a large-volume silicic magma reservoir from rapid assembly to solidification: Earth and Planetary Science Letters, v. 563, p. 1–12.

Large, S.J.E., Nathwani, C.L., Wilkinson, J.J., Knott, T R., Tapster, S.R., and Buret, Y., 2024, Tectonic and crustal processes drive multi-million year arc magma evolution leading up to porphyry copper deposit formation in central Chile: Journal of Petrology v. 65, egae023.

Lee, R.G., Dilles, J.H., Tosdal, R.M., Wooden, J.L., and Mazdab, F.K., 2017, Magmatic evolution of granodiorite intrusions at the El Salvador porphyry copper deposit, Chile, based on trace element composition and U/Pb age of zircons: Economic Geology, v. 112, p. 245–273.

Lee, R.G., Byrne, K., D'Angelo, M., Hart, C.J., Hollings, P., Gleeson, S.A., and Alfaro, M., 2021, Using zircon trace element composition to assess porphyry copper potential of the Guichon Creek batholith and Highland Valley Copper deposit, south-central British Columbia: Mineralium Deposita, v. 56, p. 215–238.

Lemne, M., 1983, Des datation K-Ar concernant surtout les magmatites subsequentes alpines des Monts Apuseni: Annual of the Institute of Geology and Geophysics, v. 61, p. 375–386.

Li, Y., Selby, D., Condon, D., and Tapster, S., 2017, Cyclic magmatic-hydrothermal evolution in porphyry systems: High-precision U-Pb and Re-Os geochronology constraints on the Tibetan Qulong porphyry Cu-Mo deposit: Economic Geology, v. 112, p. 1419–1440.

Linzer, H.G., 1996, Kinematics of retreating subduction along the Carpathian arc, Romania: Geology, v. 24, p. 167–170.

Linzer, H.G., Frisch, W., Zweigel, P., Girbacea, R., Hann, H.P., and Moser, F., 1998, Kinematic evolution of the Romanian Carpathians: Tectonophysics, v. 297, p. 133–156.

Loader, M.A., Wilkinson, J.J., and Armstrong, R.N., 2017, The effect of titanite crystallisation on Eu and Ce anomalies in zircon and its implications for the assessment of porphyry Cu deposit fertility: Earth and Planetary Science Letters, v. 472, p. 107–119.

Loader, M.A., Nathwani, C.L., Wilkinson, J.J., and Armstrong, R.N., 2022, Controls on the magnitude of Ce anomalies in zircon: Geochimica et Cosmochimica Acta, v. 328, p. 242–257.

Loucks, R.R., 2014, Distinctive composition of copper-ore-forming arcmagmas: Australian Journal of Earth Sciences, v. 61, p. 5–16.

Loucks, R.R., Fiorentini, M.L., and Henriquez, G.J., 2020, New magmatic oxybarometer using trace elements in zircon: Journal of Petrology, v. 61, p. 1–30.

Lu, Y., Loucks, R., Fiorentini, M., McCuaig, T., Evans, N.J., Yang, Z.-M., Hou, Z.-Q., Kirkland, C.L., Avila, L.P., and Kobussen, A., 2016, Zircon compositions as a pathfinder for porphyry Cu ± Mo ± Au deposits: Society of Economic Geologists, Special Publication 19, p. 329–347.

Lu, Y., Hou, Z.-Q., Yang, Z.-M., Parra-Avila, L.A., Fiorentini, M., McCuaig, T.C., and Loucks, R.R., 2017, Terrane-scale porphyry Cu fertility in the Lhasa terrane, southern Tibet [ext. abs.]: TARGET 2017, Perth, Australia, 2017, Extended Abstracts, p. 95–100.

Lukács, R., Guillong, M., Bachmann, O., Fodor, L., and Harangi, S., 2021, Tephrostratigraphy and magma evolution based on combined zircon trace element and U-Pb age data: Fingerprinting Miocene silicic pyroclastic rocks in the Pannonian Basin: Frontiers in Earth Science, v. 9, p. 1–20.

Márton, E., Tischler, M., Csontos, L., Fügenschuh, B., and Schmid, S.M., 2007, The contact zone between the ALCAPA and Tisza-Dacia megatectonic units of Northern Romania in the light of new paleomagnetic data: Swiss Journal of Geosciences, v. 100, p. 109–124.

Mason, P.R., Seghedi, I., Szákacs, A., and Downes, H., 1998, Magmatic constraints on geodynamic models of subduction in the East Carpathians, Romania: Tectonophysics, v. 297, p. 157–176.

Matenco, L., and Radivojević, D., 2012, On the formation and evolution of the Pannonian basin: Constraints derived from the structure of the junction area between the Carpathians and Dinarides: Tectonics, v. 31, p. 1–31.

Mattey, D., Lowry, D., and Macpherson, C., 1994, Oxygen isotope composition of mantle peridotite: Earth and Planetary Science Letters, v. 128, p. 231–241.

Mattinson, J.M., 2005, Zircon U-Pb chemical abrasion ("CA-TIMS") method: Combined annealing and multi-step partial dissolution analysis for improved precision and accuracy of zircon ages: Chemical Geology, v. 220, p. 47–66.

McDonough, W.F., and Sun, S., 1995, The composition of the Earth: Chemical Geology, v. 120, p. 223–253.

McLean, N.M., Bowring, J.F., and Bowring, S.A., 2011, An algorithm for U-Pb isotope dilution data reduction and uncertainty propagation: Geochemistry Geophysics Geosystems, v. 12, p. 1–26.

McLean, N.M., Condon, D.J., Schoene, B., and Bowring, S.A., 2015, Evaluating uncertainties in the calibration of isotopic reference materials and multi-element isotopic tracers (EARTHTIME tracer calibration part II): Geochimica et Cosmochimica Acta, v. 164, p. 481–501.

Merten, S., Matenco, L., Foeken, J.P.T., and Andriessen, P.A.M., 2011, Toward understanding the post-collisional evolution of an orogen influenced by convergence at adjacent plate margins: Late Cretaceous-Tertiary thermotectonic history of the Apuseni Mountains: Tectonics, v. 30, p. 1–28.

Milu, V., Leroy, J.L., and Piantone, P., 2003, The Bolcana Cu-Au ore deposit (Metaliferi Mountains, Romania): First data on the alteration and related mineralisation: Comptes Rendus Geoscience, v. 335, p. 671–680.

Milu, V., Milesi, J.P., and Leroy, J.L., 2004, Rosia Poieni copper deposit, Apuseni Mountains, Romania: Advanced argillic overprint of a porphyry system: Mineralium Deposita, v. 39, p. 173–188.

Müller, L., 2018, Geochronology and geochemistry of zircons from the Miocene magmatism and the Rovina Valley deposits—Apuseni Mountains (Romania): M.Sc. thesis, Zurich, Switzerland, ETH Zurich, 106 p.

Mungall, J.E., 2002, Roasting the mantle: Slab melting and the genesis of major Au and Au-rich Cu deposits: Geology, v. 30, p. 915–918.

Naeraa, T., Scherstén, A., Rosing, M.T., Kemp, A.I.S., Hoffmann, J.E., Kokfelt, T.F., and Whitehouse, M.J., 2012, Hafnium isotope evidence for a transition in the dynamics of continental growth 3.2 Gyr ago: Nature, v. 485, p. 627–630.

Nathwani, C.L., Simmons, A.T., Large, S.J.E., Wilkinson, J.J., Buret, Y., and Ihlenfeld, C., 2021, From long-lived batholith construction to giant porphyry copper deposit formation: Petrological and zircon chemical evolution of the Quellaveco district, southern Peru: Contributions to Mineralogy and Petrology, v. 176, p. 1–21.

Nemcok, M., Pospisil, L., Lexa, J., and Donelick, R.A., 1998, Tertiary subduction and slab break-off model of the Carpathian-Pannonian region: Tectonophysics, v. 295, p. 307–340.

Neubauer, F., Lips, A., Kouzmanov, K., Lexa, J., and Ivăşcanu, P., 2005, Subduction, slab detachment and mineralization: The Neogene in the Apuseni Mountains and Carpathians: Ore Geology Reviews, v. 27, p. 13–44.

New Senet (PTY) Ltd., 2021, NI 43-101 Technical Report on the Rovina Valley Project in Romania: Technical Report for Euro Sun Mining Inc., April 14, 2021.

Nicolae, I., and Saccani, E., 2003, Petrology and geochemistry of the Late Jurassic calc-alkaline series associated to Middle Jurassic ophiolites in the South Apuseni Mountains (Romania): Swiss Bulletin of Mineralogy and Petrology, v. 83, p. 81–96.

Nimis, P., and Omenetto, P., 2015, Does subduction polarity control metallogeny? The Mediterranean case: Terra Nova, v. 27, p. 139–146.

Pană, D.I., Heaman, L.M., Creaser, R.A., and Erdmer, P., 2002, Pre-alpine crust in the Apuseni Mountains, Romania: Insights from Sm-Nd and U-Pb data: The Journal of Geology, v. 110, p. 341–354.

Panaiotu, C., 1998, Paleomagnetic constraints on the geodynamic history of Romania: Monograph of Southern Carpathians, Reports on Geodesy, v. 7, p. 205–216.

——1999, Paleomagnetic studies in Romania: Tectonophysic implications: Ph.D. thesis, Bucharest, Romania, University of Bucharest, 150 p.

Parra-Avila, L.A., Hammerli, J., Kemp, A.I.S., Rohrlach, B., Loucks, R., Lu, Y., Williams, I.S., Martin, L., Roberts, M.P., and Fiorentini, M.L., 2022, The long-lived fertility signature of Cu-Au porphyry systems: Insights from apatite and zircon at Tampakan, Philippines: Contributions to Mineralogy and Petrology, v. 177, p. 1–22.

Paton, C., Woodhead, J.D., Hellstrom, J.C., Hergt, J.M., Greig, A., and Maas, R., 2010, Improved laser ablation U-Pb zircon geochronology through robust downhole fractionation correction: Geochemistry Geophysics Geosystems, v. 11, p. 1–36.

Paton, C., Hellstrom, J., Paul, B., Woodhead, J., and Hergt, J., 2011, Iolite: Freeware for the visualisation and processing of mass spectrometric data: Journal of Analytical Atomic Spectrometry, v. 26, p. 2508–2518.

Pătraşcu, S., Panaiotu, C., Şeclăman, M., and Panaiotu, C.E., 1994, Timing of rotational motion of Apuseni Mountains (Romania): Paleomagnetic data from Tertiary magmatic rocks: Tectonophysics, v. 233, p. 163–176.

Pearce, J.A., 1996, A user's guide to basalt discrimination diagrams. Trace element geochemistry of volcanic rocks: Application for massive sulphide exploration: Geological Association of Canada, Short Course Notes, v. 79, p. 79–113.

Pécskay, Z., Edelstein, O., Seghedi, I., Szakács, A., Kovacs, M., Crihan, M., and Bernad, A., 1995, K-Ar datings of Neogene-Quaternary calc-alkaline volcanic rocks in Romania: Acta Vulcanologica, v. 7, p. 53–61.

PEG Mining Consultants Inc., 2010, NI 43-101 Technical Report of the Rovina Exploration Property, South Apuseni Mountains, West-Central Romania: Technical Report for Carpathian Gold Inc. in collaboration with BGC Engineering Inc. and Porcupine Engineering Services Inc., April 23, 2010.

Petrus, J.A., and Kamber, B.S., 2012, VizualAge: A novel approach to laser ablation ICP-MS U-Pb geochronology data reduction: Geostandards and Geoanalytical Research, v. 36, p. 247–270.

Pettke, T., Oberli, F., and Heinrich, C.A., 2010, The magma and metal source of giant porphyry-type ore deposits, based on lead isotope microanalysis of individual fluid inclusions: Earth and Planetary Science Letters, v. 296, p. 267–277.

Reiser, M.K., Schuster, R., Spikings, R., Tropper, P., and Fügenschuh, B., 2017, From nappe stacking to exhumation: Cretaceous tectonics in the Apuseni Mountains (Romania): International Journal of Earth Sciences, v. 106, p. 659–685.

Rezeau, H., Moritz, R., Wotzlaw, J.F., Tayan, R., Melkonyan, R., Ulianov, A., Selby, D., D'Abzac, F.X., and Stern, R.A., 2016, Temporal and genetic link between incremental pluton assembly and pulsed porphyry Cu-Mo formation in accretionary orogens: Geology, v. 44, p. 627–630.

Rezeau, H., Moritz, R., Wotzlaw, J.F., Hovakimyan, S., and Tayan, R., 2019, Zircon petrochronology of the Meghri-Ordubad pluton, Lesser Caucasus: Fingerprinting igneous processes and implications for the exploration of porphyry Cu-Mo deposits: Economic Geology, v. 114, p. 1365–1388.

Richards, J., 2009, Postsubduction porphyry Cu-Au and epithermal Au deposits: Products of remelting of subduction-modified lithosphere: Geology, v. 37, p. 247–250.

——2015, Tectonic, magmatic, and metallogenic evolution of the Tethyan orogen: From subduction to collision: Ore Geology Reviews, v. 70, p. 323–345.

Roban, R.D., Ducea, M.N., Matenco, L., Panaiotu, G.C., Profeta, L., Krézsek, C., Melinte-Dobrinescu, M.N., Anastasiu, N., Dimofte, D., Apotrosoaei, V., and Francovschi, I., 2020, Lower Cretaceous provenance and sedimentary deposition in the Eastern Carpathians: Inferences for the evolution of the subducted oceanic domain and its European passive continental margin: Tectonics, v. 39, p. 1–28.

Roban, R.D., Ducea, M.N., Mihalcea, V.I., Munteanu, I., Barbu, V., Melinte-Dobrinescu, M.C., Olariu, C., and Vlăsceanu, M., 2023, Provenance of Oligocene lithic and quartz arenites of the East Carpathians: Understanding sediment routing systems on compressional basin margins: Basin Research, v. 35, p. 244–270.

Rocha, V.S., 2013, Geochronology and magma geochemistry of Au-rich porphyry deposits at Rovina, Colnic and Ciresata (South Apuseni Mts., Romania): M.Sc. thesis, Zurich, Switzerland, ETH Zurich, 67 p.

Rohrlach, B.D., Loucks, R.R., and Porter, T.M., 2005, Multi-million-year cyclic ramp-up of volatiles in a lower crustal magma reservoir trapped below the Tampakan copper-gold deposit by Mio-Pliocene crustal compression in the southern Philippines, *in* Porter, T.M., ed., Super porphyry copper and gold deposits: A global perspective, v. 2: Adelaide, PCG Publishing, p. 369–407.

Ross, P.S., and Bédard, J.H., 2009, Magmatic affinity of modern and ancient subalkaline volcanic rocks determined from trace-element discriminant diagrams: Canadian Journal of Earth Sciences, v. 46, p. 823–839.

Roşu, E., 2001, Geological map of the South Apuseni Mts, Alpine magmatism and related ore deposits: Romanian Journal of Mineral Deposits, v. 79, scale 1:225,000.

Roşu, E., Pécskay, Z., Ştefan, A., Popescu, G., Panaiotu, C., and Panaiotu, C.E., 1997, The evolution of the Neogene volcanism in the Apuseni Mountains (Romania): Constraints from new K-Ar data: Geologica Carpathica, v. 48, p. 353–359.

Roşu, E., Szakács, A., Downes, H., Seghedi, I., Pécskay, Z., and Panaiotu, C., 2001, The origin of Neogene calc-alkaline and alkaline magmas in the Apuseni Mountains, Romania: The adakite connection: Romanian Journal of Minereral Deposits, v. 71, p. 3–23.

Roşu, E., Seghedi, I., Downes, H., Alderton, D.H., Szakács, A., Pécskay, Z., Panaiotu, C., Panaiotu, C.E., and Nedelcu, L., 2004a, Extension-related Miocene calc-alkaline magmatism in the Apuseni Mountains, Romania: Origin of magmas: Swiss Bulletin of Mineralogy and Petrology, v. 84, p. 153–172.

Roşu, E., Udubasa, G., Pécskay, Z., Panaiotu, C., and Panaiotu, C.E., 2004b, Timing of Miocene-Quaternary magmatism and metallogeny in the south Apuseni mountains, Romania: Romanian Journal of Mineral Deposits, v. 81, p. 33–38.

Ruff, R., 2013, The Rovina Valley Au-Cu project, Golden Quadrilateral, Romania: New discoveries in an old mining district: Toronto Geological Discussion Group, Carpathian Gold Inc., Toronto, April 16, 2013, Presentation.

Ruff, R.K., Stefanini, B., and Halga, S., 2012, Geology and petrography of the gold-rich Ciresata porphyry deposit, Metaliferi Mountains, Romania: Romanian Journal of Mineral Deposits, v. 85, p. 19–24.

Săndulescu, M., 1984, Geotectonics of Romania: Romania, Editura Tehnică Bucharest, 334 p. (in Romanian).

Schaltegger, U., and Davis, J.H.F.L., 2017, Petrochronology of zircon and baddeleyite in igneous rocks: Reconstructing magmatic processes at high temporal resolution: Reviews in Mineralogy and Geochemistry, v. 83, p. 297–328.

Schaltegger, U., Brack, P., Ovtcharova, M., Peytcheva, I., Schoene, B., Stracke, A., Marocchi, M., and Bargossi, G.M., 2009, Zircon and titanite recording 1.5 million years of magma accretion, crystallization and initial cooling in a composite pluton (southern Adamello batholith, northern Italy): Earth and Planetary Science Letters, v. 286, p. 208–218.

Scherer, E., Munker, C., and Mezger, K., 2001, Calibration of the lutetium-hafnium clock: Science, v. 293, p. 683–687.

Schmid, S.M., Bernoulli, D., Fügenschuh, B., Matenco, L., Schefer, S., Schuster, R., Tischler, M., and Ustaszewski, K., 2008, The Alpine-Carpathian-Dinaridic orogenic system: Correlation and evolution of tectonic units: Swiss Journal of Geosciences, v. 101, p. 139–183.

Schmid, S.M., Fügenschuh, B., Kounov, A., Maţenco, L., Nievergelt, P., Oberhänsli, R., Pleuger, J., Schefer, S., Schuster, R., Tomljenović, B.,

Ustaszewski, K., and Van Hinsbergen, D.J., 2020, Tectonic units of the Alpine collision zone between Eastern Alps and western Turkey: Gondwana Research, v. 78, p. 308–374.
Schoene, B., and Baxter, E.F., 2017, Petrochronology and TIMS: Reviews in Mineralogy and Geochemistry, v. 83, p. 231–260.
Seghedi, I., 2004, Geological evolution of the Apuseni Mountains with emphasis on the Neogene magmatism—a review Romania (Guidebook of the International Field Workshop of IGCP project 486): International Association on the Genesis of Ore Deposits (IAGOD) Guidebook Series, v. 11, p. 5–23.
Seghedi, I., Bojar, A.V., Downes, H., Roşu, E., Tonarini, S., and Mason, P., 2007, Generation of normal and adakite-like calc-alkaline magmas in a non-subductional environment: An Sr-O-H isotopic study of the Apuseni Mountains neogene magmatic province, Romania: Chemical Geology, v. 245, p. 70–88.
Seghedi, I., Ntaflos, T., Pécskay, Z., Panaiotu, C., Mirea, V., and Downes, H., 2022, Miocene extension and magma generation in the Apuseni Mts. (western Romania): A review: International Geology Review, v. 64, p. 1–27.
Sillitoe, R.H., 2010, Porphyry copper systems: Economic Geology, v. 105, p. 3–41.
Sperner, B., Ratschbacher, L., and Nemčok, M., 2002, Interplay between subduction retreat and lateral extrusion: Tectonics of the Western Carpathians: Tectonics, v. 21, p. 1–24.
Stoica, A.M., Ducea, M.N., Roban, R.D., and Jianu, D., 2016, Origin and evolution of the South Carpathians basement (Romania): A zircon and monazite geochronologic study of its Alpine sedimentary cover: International Geology Review, v. 58, p. 510–524.
Storck, J.C., Laurent, O., Karakas, O., Wotzlaw, J.F., Galli, A., Sinigoi, S., Bachmann, O., and Chelle-Michou, C., 2021, Mantle versus crustal contributions in crustal-scale magmatic systems (Sesia magmatic system, northern Italy) from coupling Hf isotopes and numerical modelling: Contributions to Mineralogy and Petrology, v. 176, p. 1–19.
Szymanowski, D., Fehr, M.A., Guillong, M., Coble, M.A., Wotzlaw, J.F., Nasdala, L., Ellis, B., Bachmann, O., and Schönbächler, M., 2018, Isotope-dilution anchoring of zircon reference materials for accurate Ti-in-zircon thermometry: Chemical Geology, v. 481, p. 146–154.
Takács, E., Szalay, I., Bodoky, T., Hegedüs, E., Kántor, J., Timár, Z., Varga, G., Bérczi, I., Szalay, A., Nagy, Z., et al., 1996, International deep reflection survey along the Hungarian Geotraverse: Geophysical Transactions, v. 40, p. 1–44.
Tapster, S., Condon, D.J., Naden, J., Noble, S.R., Petterson, M.G., Roberts, N.M.W., Saunders, A.D., and Smith, D.J., 2016, Rapid thermal rejuvenation of high-crystallinity magma linked to porphyry copper deposit formation; evidence from the Koloula porphyry prospect, Solomon Islands: Earth and Planetary Science Letters, v. 442, p. 206–217.
Tischler, M., Gröger, H.R., Fügenschuh, B., and Schmid, S.M., 2007, Miocene tectonics of the Maramures area (Northern Romania): Implications for the Mid-Hungarian fault zone: International Journal of Earth Sciences, v. 96, p. 473–496.
Trail, D., Watson, E.B., and Tailby, N.D., 2012, Ce and Eu anomalies in zircon as proxies for the oxidation state of magmas: Geochimica et Cosmochimica Acta, v. 97, p. 70–87.
Tusa, L., Andreani, L., Khodadadzadeh, M., Contreras, C., Ivascanu, P., Gloaguen, R., and Gutzmer, J., 2019, Mineral mapping and vein detection in hyperspectral drill-core scans: Application to porphyry-type mineralization: Minerals, v. 9, article 122.
Udubaşa, G., Roşu, E., Seghedi, I., and Ivăşcanu, P.M., 2001, The "Golden Quadrangle" in the Metaliferi Mts., Romania: What does this really mean?: Romanian Journal of Mineral Deposits, v. 79, p. 24–35.
Ustaszewski, K., Schmid, S.M., Fügenschuh, B., Tischler, M., Kissling, E., and Spakman, W., 2008, A map-view restoration of the Alpine-Carpathian-Dinaridic system for the Early Miocene: Swiss Journal of Geosciences, v. 101, p. S273-S294.
van Hinsbergen, D.J., Torsvik, T.H., Schmid, S.M., Matenco, L.C., Maffione, M., Vissers, R.L., Gürer, D., and Spakman, W., 2020, Orogenic architecture of the Mediterranean region and kinematic reconstruction of its tectonic evolution since the Triassic: Gondwana Research, v. 81, p. 79–229.
Vermeesch, P., 2018, IsoplotR: A free and open toolbox for geochronology: Geoscience Frontiers, v. 9, p. 1479–1493.
——2021, On the treatment of discordant detrital zircon U-Pb data: Geochronology, v. 3, p. 247–257.
Vlad, Ş.N., and Orlandea, E., 2004, Metallogeny of the Gold quadrilateral: Style and characteristics of epithermal-subvolcanic mineralized structures, South Apuseni Mts., Romania: Studia UBB Geologia, v. 49, p. 15–31.
von Quadt, A., Moritz, R., Peytcheva, I., and Heinrich, C.A., 2005, Geochonology and geodynamics of Late Cretaceous magmatism and Cu-Au mineralization in the Panagyurishte region of the Apuseni-Banat-Timok-Snednogorie belt, Bulgaria: Ore Geology Reviews, v. 27, p. 95–126.
von Quadt, A., Erni, M., Martinek, K., Moll, M., Peytcheva, I., and Heinrich, C.A., 2011, Zircon crystallization and the lifetimes of ore-forming magmatic-hydrothermal systems: Geology, v. 39, p. 731–734.
von Quadt, A., Gallhofer, D., Guillong, M., Peytcheva, I., Waelle, M., and Sakata, S., 2014, U-Pb dating of CA/non-CA treated zircons obtained by LA-ICP-MS and CA-TIMS techniques: Impact for their geological interpretation: Journal of Analytical Atomic Spectrometry, v. 29, p. 1618–1629.
von Quadt, A., Wotzlaw, J.F., Buret, Y., Large, S.J., Peytcheva, I., and Trinquier, A., 2016, High-precision zircon U/Pb geochronology by ID-TIMS using new 10^{13} ohm resistors: Journal of Analytical Atomic Spectrometry, v. 31, p. 658–665.
Winchester, J.A., and Floyd, P.A., 1977, Geochemical discrimination of different magma series and their differentiation products using immobile elements: Chemical Geology, v. 20, p. 325–343.
Wortel, M.J.R., and Spakman, W., 2000, Subduction and slab detachment in the Mediterranean-Carpathian region: Science, v. 290, p. 1910–1917.
Wotzlaw, J.F., Hüsing, S.K., Hilgen, F.J., and Schaltegger, U., 2014, High-precision zircon U-Pb geochronology of astronomically dated volcanic ash beds from the Mediterranean Miocene: Earth and Planetary Science Letters, v. 407, p. 19–34.
Wotzlaw, J.F., Buret, Y., Large, S.J.E., Szymanowski, D., and von Quadt, A., 2017, ID-TIMS U-Pb geochronology at the 0.1 parts per thousand level using 10^{13} Ω resistors and simultaneous U and $^{18}O/^{16}O$ isotope ratio determination for accurate UO_2 interference correction: Journal of Analytical Atomic Spectrometry, v. 32, p. 579–586.
Zimmerman, A., Stein, H.J., Hannah, J.L., Koželj, D., Bogdanov, K., and Berza, T., 2008, Tectonic configuration of the Apuseni-Banat-Timok-Srednogorie belt, Balkans-South Carpathians, constrained by high precision Re-Os molybdenite ages: Mineralium Deposita, v. 43, p. 1–21.

Sava Markovic is currently pursuing a Ph.D. degree in the Mineral Resource Systems group at ETH Zurich (Switzerland). His current research combines field work with high-precision zircon geochronology in exploring the dynamics of Sn mineralization in peraluminous granitic systems of the Peruvian Eastern Cordillera. He previously worked on several Cu-Au porphyry deposits of the Late Cretaceous-Neogene Apuseni-Banat-Timok-Srednogorie belt in the Balkans. Sava obtained his B.Sc. degree in geology from his hometown University of Belgrade (Serbia) and holds an M.Sc. degree from ETH Zurich.